NOTICE

The quality of this microfiche is heavily dependent upon the quality of the original thesis submitted for microfilming. Every effort has been made to ensure the highest quality of reproduction possible.

If pages are missing, contact the university which granted the degree.

Some pages may have indistinct print especially if the original pages were typed with a poor typewriter ribbon or if the university sent us a poor photocopy.

Previously copyrighted materials (journal articles, published tests, etc.) are not filmed.

Reproduction in full or in part of this film is governed by the Canadian Copyright Act, R.S.C. 1970, c. C-30. Please read the authorization forms which accompany this thesis.

AVIS

La qualité de cette microfiche dépend grandement de la qualité de la thèse soumise au microfilmage. Nous avons tout fait pour assurer une qualité supérieure de reproduction.

S'il manque des pages, veuillez communiquer avec l'université qui a conféré le grade.

La qualité d'impression de certaines pages peut laisser à désirer, surtout si les pages originales ont été dactylographiées à l'aide d'un ruban usé ou si l'université nous a fait parvenir une photocopie de mauvaise qualité.

Les documents qui font déjà l'objet d'un droit d'auteur (articles de revue, examens publiés, etc.) ne sont pas microfilmés.

La reproduction, même partielle, de ce microfilm est soumise à la Loi canadienne sur le droit d'auteur, SRC 1970, c. C-30. Veuillez prendre connaissance des formules d'autorisation qui accompagnent cette thèse.

THIS DISSERTATION
HAS BEEN MICROFILMED
EXACTLY AS RECEIVED

LA THÈSE A ÉTÉ
MICROFILMÉE TELLE QUE
NOUS L'AVONS REÇUE

A Digital System for Measurement of Resonant Frequency and Q factor .

by

Rajani Kanth Pandrangi

A thesis
presented to University of Ottawa
in partial fulfillment of the
requirements for the degree of
M.A.Sc.
in
Department of Electrical Engineering

Ottawa, Ontario, 1981

ABSTRACT

In this thesis , a new on-line system for the measurement of resonant frequency and Q factor is described.The existing systems are reviewed; this is followed by a description of certain theoretical aspects ,the principle of operation and advantages of the new system.The experimental arrangement is presented followed by a description of the system simulation. Finally , the performance of the measurement system is outlined.

ACKNOWLEDGEMENTS

The author wishes to express his gratitude to his supervisor , Professor S.S.Stuchly , for his guidance throughout the course of this research.

Thanks are also due to other members of the Department of Electrical Engineering , especially Mohammed Master , Benito Carraro and Steve Symons for their invaluable assistance in the execution of this project. The financial support for this research by the National Sciences and Engineering Research Council of Canada and the Ontario Ministry of Labour is greatly appreciated.

LIST OF TABLES

LIST OF FIGURES

LIST OF SYMBOLS.

β_1 , β_2	The input and output coupling coefficients of the resonator
Δc	The absolute uncertainity of the frequency counter
Δf_A	The absolute uncertainity resulting from the algorithm used to determine the inflection points
Δf_{VCO}	The absolute uncertainity in the VCO frequency
$\Delta V_o(f)$	The change in the output signal corresponding to a single frequency increment.
Δf_k	The random frequency of the k th sample point used in the simulation
e_{t3}	The truncation error of the first derivative using the 3-point Lagrangian interpolation polynomial
e_{t5}	The truncation error of the first derivative using the 5-point Lagrangian interpolation polynomial using equally spaced points
f_o	The resonant frequency
f_1 , f_2	The first and second inflection points
f/V	The frequency/voltage characteristic of the VCO
f'_k	The extrapolated sample frequency obtained from the f/V characteristic , used in the simulation

f_{start}	The initial value of frequency used in the extrapolation to obtain f'_k
K_1	The slope of the linear f/V characteristic of the VCO
K_2	The slope of the linear P/f characteristic of the VCO
K_3	The detector sensitivity
N/S	The noise to signal voltage ratio
P/f	The power/frequency characteristic of the VCO
$P_{in.k}$	The VCO signal power level at the k th sample point
$P_{in.0}$	The initial value of the signal power level used in the extrapolation of $P_{in.k}$ from the P/f characteristic
$P_{0.k}$	The resonator output power corresponding to the k th sample point
Q factor	The quality factor
q	The quantization error of an A/D converter
r	The resolution of the D/A converter
S	The slope of the VCO V/f characteristic
S/N	The signal to noise voltage ratio
$V_{in}(f)$	The detected voltage at the input of the resonator
$V_0(f)_{max}$	The maximum detected voltage at the output of the resonator
V_k	The tuning voltage of the k th sample point
$V_{in.k}$	The detector output voltage of the k th sample

	point corresponding to $P_{in\cdot k}$
$V_{o\cdot k}$	The detector output voltage of the k th sample
	point corresponding to $P_{o\cdot k}$
VCO	Voltage controlled oscillator

CONTENTS

Chapter I

INTRODUCTION

The need for accurate determination of resonant frequency and Q factor of resonant structures arises from the use of radio frequency (RF) and microwave (MW) resonators in continuous monitoring of electric and non-electric parameters[1].

The resonators are used as sensors, particularly in inaccessible conditions such as extreme temperatures, intense radiation, large electric and magnetic fields, etc.

The resonant frequency of the resonator is a function of the measured non-electric quantity and, if monitored continuously, provides continuous information about that quantity.

Accurate knowledge of resonant frequency and Q factor is also required in applications such as measurements of dielectric and magnetic properties of materials, determinations of absolute intensities of spectroscopic lines and the design of electronic devices [1].

Typical applications of resonators in non-electric parameter monitoring include monitoring moisture content, liquid hydrogen density, size and volume of food products, temperature in nuclear reactors and cryogenics, and in

measurements of diameter of dielectric fibres and metal wires [1].

In addition, when conventional methods (such as evaluation of permittivities from reflection coefficient measurements) are used to measure the permittivity of lossy materials such as biological tissues, the uncertainities of experimental measurement increase rapidly [2] for materials with larger dielectric constants ($\varepsilon > 10$) and lossy materials ($\tan\delta > 0.1$). In such cases a resonator can be used and the permittivity can be inferred from experimental evaluation of resonant frequncy and Q factor of the resonator.

This thesis dealt with the development of a new automated system for the measurement of resonant frequency and Q factor. This system was intended for use in monitoring dielectric properties of materials. The system is not, however, dependant on the area of application. The following sections provide an outline of the work that comprised this thesis.

Chapter II consists of a comparative study of existing systems for resonant frequency and Q factor measurement; important features of the systems such as measurement accuracies, frequencies of operation, mode of measurment (manual or automated) as well as a brief description of the measurement technique are provided.

Chapter III deals with certain theoretical aspects;the principles of operation of the new measurement system and its advantages are enumerated. An estimate of the theoretical measurement uncertainity is obtained.

Chapter IV provides a description of the experimental arrangement.The measurement process is detailed , followed by the system hardware and software. The hardware section describes the equipment used while the software section deals with the algorithms and the programs used.

A simulation of the measurement system is presented in Chapter V.The simulation was used to investigate the effects of VCO uncertainities and signal/noise ratios on the measurement system , since these factors were considered to affect the measurement uncertainity most.

Chapter VI describes the performance of the measurement system.The system was tested on a coaxial resonator whose resonant frequency and Q factor were variable.The system was tested at different frequencies and for different Q factors;statistical variations of the measured parameters were computed. An analysis of the usefullness of the measurement system for the intended areas of application were then considered followed by a study of the factors affecting the experimental measurement uncertainities.

Finally , conclusions are presented in Chapter VII , detailing the evolution of the system including the various stages of execution of this project , the intended design objectives and the extent to which these objectives were satisfied.

Chapter II

Q FACTOR MEASUREMENT TECHNIQUES.

Table 1 shows the different Q factor measurement techniques.

TABLE 1

Q factor measurement techniques.

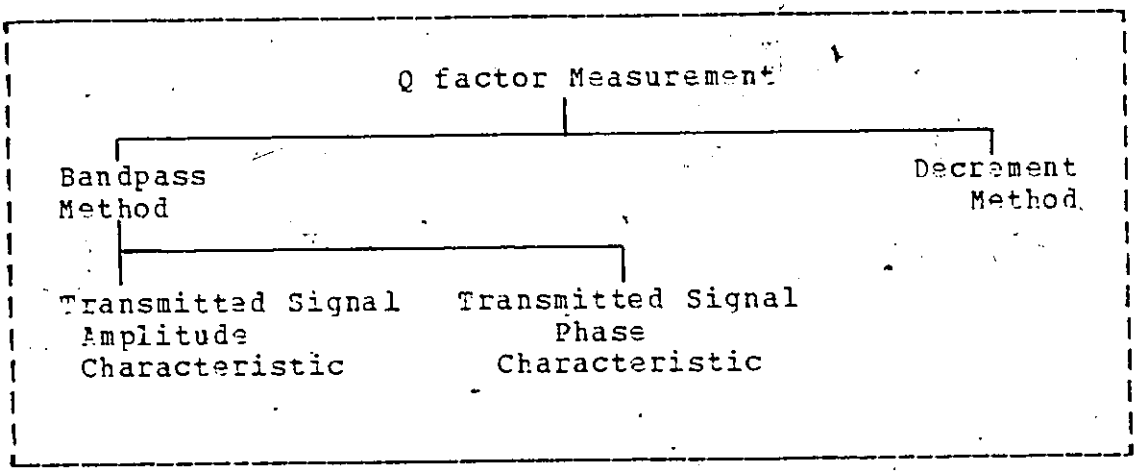

The two general methods [3] are :

(1) Bandpass method.

(2) Decrement method.

The bandpass method analyzes the response of the resonator to CW signals around resonance.The measurements can

be made either point-by-point or by a frequency sweep technique. Among the various bandpass techniques, the transmitted-signal- amplitude and phase-characteristic-based techniques are used widely. These methods are, however, unsuitable for measurement of high values of Q owing to the frequency instability of the signal sources.

The decrement method is particularly suitable for measurement of high values of Q: 10^5 to 10^9. This method uses the transient response of the circuit to a sudden application or removal of an exciting signal at a frequency close to the resonant frequency. However, as the Q value decreases, measurements of short time intervals required in this method become more difficult [4]. Chirkov & Kozak however, presented [13] a measurement technique using the decrement method for lower Qs of the order of 5. The method will be considered in greater detail later.

Further classification of Q factor measurement techniques can be made in terms of whether the control and processing is done using analog or digital techniques.

Analog techniques of Q factor measurement have been documented quite extensively in [3] & [4]. Some more recent approaches, particularly automated systems, are described here, along with digital measurement techniques. Table 2 compares the relative uncertainities of the different measurement techniques.

TABLE 2

Comparison of existing systems for Q factor measurement.

		Method	Author Name & reference	Operating frequency	Measurable Q	Measurement Accuracy
Analog	Manual	Amplitude Characteristic	Francis [5]	< 1GHZ	100-10,000	6% to 26%
			Kneppo [6]	X Band	7000	Not specified.
		Transmitted Signal Phase Characteristic	Cullen & Davies [7]	X Band	10,000-100,000	1%
		Other	Kneppo [8]	X Band	7000 to 11,000	5%
	Automated	Amplitude Characteristic	Miller [9]	X Band	7000	0.1%
			Hey & Gardiol [10]	Microwave	10000	2%
			Eugene & Mollet [11]	9 GHZ	A few thousand	A few percent
		Transmitted Signal Phase Characteristic	Linzer&Stokesberry [12]	X Band	7000	5%
Digital	Automated	Decrement Method	Chirkov & Kozak [13]	Low freq.	<5	2%
		Energy in reactive and resistive components.	Popovic [14]	400kHZ-600kHZ	30 to 100	2.5%
		Transmitted Signal Phase Characteristic	Akyel & Bosisio [15]	Microwave	Variations of Q in 500-7000 range	± 1.2%

2.1 ANALOG METHODS.

These are classified into manually-operated systems and automated systems.

2.1.1 Manually-operated Systems.

Manually-operated systems can be further divided as follows:

(1) Transmitted-Signal-Amplitude-Characteristic-Based Systems

(2) Transmitted-Signal-Phase-Characteristic-Based Systems

(3) Other Systems

2.1.1.1 Transmitted-Signal-Amplitude-Characteristic-Based Systems.

Francis [5] described a method of measuring the Q factor, the capacitance and the series resistance of capacitors in the 100-10,000 range at frequencies below 1 GHz with accuracies of about six to twenty six percent. The test capacitor was connected in series or in shunt to a resonant coaxial line whose characteristics were known; the measured Q factor of the combination was used along with the known Q factor of the resonant line to determine the Q factor of the test capacitor. The parameters of the test capacitor were evaluated from the measurement of two frequencies one on either

side of the resonator response at a pre-determined ratio of resonant to off-resonant voltage. This method requires a signal generator with excellent frequency stability, as well as a highly accurate detector and a frequency counter.

Kneppo [6] presented a comparison method of measuring the Q factor. The difference between the transmitted signal of a test resonator and a reference resonator was displayed on the Y-axis of an oscilloscope; the transmitted signal of the reference resonator was recorded on the X-axis. The shape of the displayed curve depends on the difference in parameters of both resonators and the displayed data was used to calculate the Q factor of the test resonator.

The author feels that this method is extremely sensitive to small changes in the Q factor. It requires a stable, level-controlled sweep generator, linear microwave power meters and (manual) measurement of difference in transmitted signal on a calibrated oscilloscope.

2.1.1.2 Transmitted-Signal-Phase-Characteristic-Based Systems.

Cullen & Davies [7] described a method of measuring the Q factor in the 10^4 to 10^5 range in the X-band, with an estimated accuracy of 1%. The system used a phase lockin system to obtain ± 45 ° points on the resonance curve to a high degree of accuracy - by measuring the phase shift at a

constant intermediate frequency(IF). The ± 45 ° phase shift in the source signal transmitted through the resonator was compared with a ± 45 ° phase shift produced at the intermediate frequency by a harmonically-locked phase shifting technique.

This method can be used to measure the loss tangent of a low-loss dielectric material.The loss tangent is determined by measuring the loaded and unloaded Q factor of an open resonator.

2.1.1.3 Other Systems.

Kneppo [8] also described a technique which used the integral of the resonance curve around resonance of a transmission type cavity to calculate the Q factor. The integral of the transmitted power of the cavity over a known interval was related to the Q factor and the latter was calculated from a knowledge of the transmitted power at resonance , the resonant frequency and the integration interval.The system was tested with two cavities with Q factors of 7500 and 11,750 with an accuracy of about five percent. The main advantage is that the equipment required is simple, and precise measurements of 3-dB frequencies - as used in transmission characteristic methods - are not necessary.

2.1.2. Automated Systems.

The degree of automation of the measurement process, among the systems considered here, varies from automation of bandwidth measurement - to total automation yielding the computed values of the Q factor and the resonant frequency from the measured parameters.

As before the measurement systems can be classified in terms of whether the transmitted signal amplitude or phase characteristic are being used.

2.1.2.1 Transmitted-Signal-Amplitude-Characteristic-Based Systems.

Miller [9] used a VCO operating in an automatic frequency control (AFC) loop to obtain the resonant frequency of a test cavity;a 3-dB attenuator was then inserted into the line .The detected output was fed to the difference output of a comparison circuit and the amplified output was reduced to zero by means of a reference voltage.Removing the 3-dB attenuation causes the amplifier to drive the VCO in the AFC loop to a frequency at which the detected output equals that of the reference voltage.The other 3-dB point was obtained by introducing a 180 phase change in the loop.

Accuracies of the Q factor better than 0.1% for a high Q resonator with a Q of about 7000 are reported.

Ney & Gardiol [10] proposed an automatic cavity monitor which measures the resonant frequency and loaded Q factor. Q factors below 1000 can be measured with an accuracy better than 2%.

A sweep oscillator was used to sweep between two points on the resonance curve of the cavity and pulses corresponding to the 3-dB banwidth (DEL F) and the difference (F2-Fr) between the sweep end point -F2- and the resonance frequency Fr were obtained; these pulses were then smoothed and Fr and DEL F were determined by a calibrated wavemeter.

Eugene & Mollat [11] reported an automatic device capable of operating at 9 GHZ and determining the Q factor to within a few percent. The resonant frequency is measured to within 100 ppm.

This method uses the principle of locking a VCO to the peak of the resonance curve and to the 3-dB points and determining the Q factor from the frequencies obtained.

This device was used for dielectric measurements using the cavity perturbation technique.

2.1.2.2 Transmitted-Signal-Phase-Characteristic-Based Systems.

Linzer & Stokesberry [12] described a system for measurement of the Q factor of reflection and transmission

type cavities in the X band. The authors claimed that the system was :

(1) highly accurate and fast

(2) independant of source frequency

(3) readily automated

(4) suitable for measurement of low as well as high Qs of either transmission or reflection type cavities.

and (5) capable of measuring very small changes in Q

Using their system a manufacturer - specified Q of 7000 has been measured with an accuracy better than 5% and changes in Q are detectable with accuracies of 1%.

The method used the information contained in the phase shift of the resonator as a function of frequency; an oscillator was used to lock in to some point away from the centre of the resonance curve;this fractional frequency shift from the centre depends on the loaded Q factor of the cavity as well as a known phase offset used to obtain the fractional frequency shift. The Q factor was then evaluated from the phase and frequency shifts.

2.2 DIGITAL TECHNIQUES.

Information on digital techniques for Q factor measurements is somewhat scarce. Chirkov & Kozak [13] proposed a low frequency digital Q meter,for tuned circuits with Q factors of less than 5 and measurement accuracies of 2%. Their system used the decrement method.

Popvic [14] proposed a method of digitally measuring Q for frequencies between 400 kHZ to 600 kHZ and a Q range of 30 to 100 determined with an accuracy of 2.5%. Their system related the ratio of the tuned circuit voltage output at resonance and the corresponding input voltage to the Q factor; pulses proportional to these two voltages at resonance were obtained and the Q factor was evaluated from the corresponding frequencies or time periods.

Akyel & Bosisio [15] described a microprocessor-controlled digital technique for measurements of the resonant frequency deviations of 20 MHZ ± 2.5% and Q factor variations in the 500-7000 range with an accuracy better than 1.2%. This system was designed to record the changes of the resonant frequency and the Q factor when a resonant cavity was perturbed.

The phase-characteristic of a transmission type resonator was used. The system operated as follows : an electronic phase shifter introduced a periodic phase shift inside a closed loop containing the cavity, a variable attenuator, an electronic phase shifter and a microprocessor-controlled mechanical phase shifter.The corresponding frequency was measured by a frequency counter connected to the system through the IEEE 488 bus.The microprocessor then adjusted the mechanical phase shifter so as to minimize the amplitude of the measured frequency shift. At this setting of the closed

loop system the average frequency (F0) and the frequency shift (DEL F0) were used to calculate the loaded Q factor of the perturbed cavity, the Q factor of the unperturbed cavity being known.

Akyel & Bosisio also described [16] a method of measuring Q under microprocessor control and using it in the calculation of the permittivity of materials.

Chapter III

THEORY

3.1 BASIC DEFINITIONS.

The Q factor of a resonant circuit is a measure of the energy stored and dissipated :

$$Q = 2\pi \frac{\text{Energy stored in the system}}{\text{Energy dissipated in the system per cycle}} \qquad (3.1)$$

A resonator near resonance can be represented by a simple series or parallel resonant circuit [3]. This representation refers to certain reference planes in the input and output transmission lines viz., a voltage node (standing wave minimum) or a voltage antinode (standing wave maximum).

Figure 1 shows the equivalent circuit representation of a resonator at a voltage antinode. The Q factor can be calculated from the energy stored and dissipated in the circuit. Accordingly, three different kinds of Q factors are defined, depending on the circuit used in the calculation of the dissipated energy.

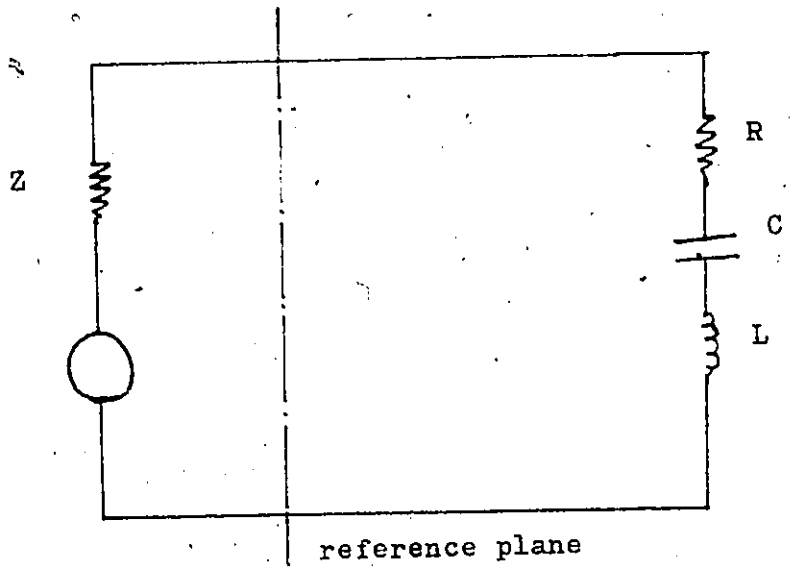

Figure 1: Equivalent circuit representation of a resonator at a voltage antinode.

The unloaded Q factor (Q_o) includes only the losses of the resonator in the calculation of the dissipated energy. Thus

$$Q_o = \frac{\omega_o L I^2/2}{I^2 R/2} = \frac{\omega_o L}{R} \qquad (3.2)$$

where ω_o is the resonant frequency and the other symbols are defined in Figure 1

The loaded Q factor (Q_L) includes all sources of dissipation in the circuit :

$$Q_L = \frac{\omega_o L I^2/2}{I^2(R+Z_o)/2} = \frac{\omega_o L}{R + Z_o} \qquad (3.3)$$

The external Q factor (Q_{ex}) accounts only for the external losses :

$$Q_{ex} = \frac{\omega_o L I^2/2}{I^2 Z_o/2} = \frac{\omega_o L}{Z_o} \qquad (3.4)$$

Defining Z_o/R as the coupling parameter (β)

$$Q_L = Q_o/(1+\beta) \qquad (3.5)$$

$$Q_{ex} = Q_o/\beta \qquad (3.6)$$

The coupling parameter (β) is a measure of the efficiency with which the energy stored in the resonator is coupled to the external load and dissipated there.

Figure 2 shows a cavity coupling system consisting of a generator with $R_g = Z_o$ coupled to the resonator input and a load $R_L = Z_o$ coupled to the resonator output. Figure 3 depicts an equivalent circuit with the resonator represented by a series resonant circuit and the coupling circuits by ideal transformers of turns ratio n_1 and n_2. Figure 4 shows the circuit with input and output resistances transformed to the centre loop.

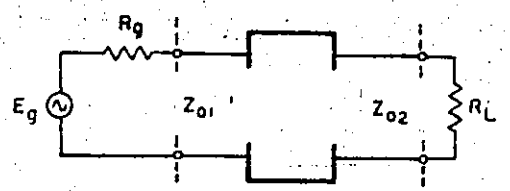

Figure 2: Transmission-type resonator with input and output transmission lines.

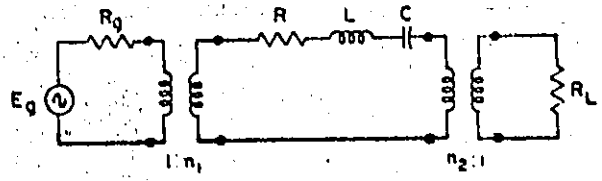

Figure 3: Equivalent circuit representation of the resonator from Fig.2.

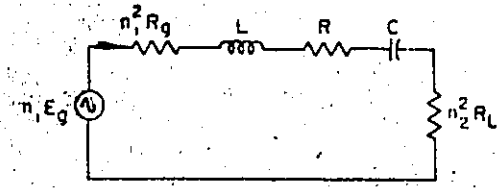

Figure 4: The circuit from Fig.3 with the impedance transformed to the middle loop.

The transmission loss $T(\omega)$ between the input and output ports of a resonator , is given by :

$$T(\omega) = \frac{P_0}{P_{in}} = \frac{4\beta_1\beta_2}{(1+\beta_1+\beta_2)^2 + 4Q_L^2\left(\frac{\delta\omega}{\omega_0}\right)^2}$$

where :

P_0 is the output power

P_{in} is the input power

$\delta w = w - w_0$, while $w = 2\pi f$ is the angular frequency and w_0 is the angular resonant frequency.

β_1 and β_2 are the input and output coupling coefficients with $\beta_1 = n_1^2 R_g/Z_0$ and $\beta_2 = n_2^2 R_L^2/Z_0$.

At resonance , maximum power is transmitted and ,

$$T(\omega_0) = \frac{4\beta_1\beta_2}{(1+\beta_1+\beta_2)^2}$$

The normalized transmission loss is :

$$\frac{T(\omega)}{T(\omega_0)} = \frac{1}{\left(1 + 4Q_L^2(\delta\omega/\omega_0)^2\right)}$$

or

$$\frac{T(f)}{T(f_0)} = \frac{1}{\left(1 + 4Q_L^2(\delta f/f_0)^2\right)} \qquad (3.7)$$

where $\delta f = f - f_0$ and f_0 is the resonant frequency.

The inflection points on the resonance curve can be determined by obtaining $T''(f)$ from (3.7) and equating it to zero. Thus ,

$$\frac{2Q_L(f_{1/2} - f_0)}{f_0} = \pm \frac{1}{\sqrt{3}} \qquad (3.8)$$

where $f_{1/2}$ are the frequencies corresponding to the first and second inflection points . The inflection points are as-

sumed to lie symmetrically about the resonant frequency. Thus ,

$$f_0 = \frac{f_1 + f_2}{2} \qquad (3.9)$$

From (3.8) and (3.9) , therefore ,

$$Q_L = \frac{f_1 + f_2}{2\sqrt{3}\,(f_2 - f_1)} \qquad (3.10)$$

In this way , the resonant frequency and Q factor are obtained in terms of the inflection point frequencies of the resonance curve.

3.2 PRINCIPLE OF OPERATION.

Systems used for measurement of the Q factor generally make use of frequency sweep techniques to obtain the resonant structure response as a continuous function of frequency [1]-[16].These systems usually detect the transmitted power at resonance as well as at the 3-dB or inflection points on the resonance curve.This feature makes these systems dependant on the detector characteristic.In addition relative flatness of the resonance curve in the vicinity of resonance makes it difficult to estimate the resonant frequency and hence Q factor accurately.Also ,if the measurement process is slow, source signal instabilities (such as frequency and power level instabilities) may cause additional errors. This latter problem also occurs in systems utilizing the phase characteristic . Moreover , these systems require precise measurements of the 3-dB bandwidth which is difficult especially for high-Q cavities. These problems also occur in inflection-point techniques based on

measurements utilizing the linearity of the detected output at the inflection points [3].

A different approach is taken in the proposed system. In this system , the inflection points on the resonance curve are identified through a process of mathematical evaluation .At the inflection points the second derivative is equal to zero while the first derivative reaches maximum positive or negative values . By identifying therefore , the points on the resonance curve at which the positive and negative derivative maxima occur, the inflection points can be located.

The system operates as follows . The resonator frequency response is sampled ,under computer control, over a certain range of frequencies and the samples are digitized and stored in the computer memory,along with the corresponding frequencies which are measured with a digital counter interfaced directly to the computer. Numerical techniques are applied to the sampled data to identify the inflection points on the resonance curve. Once the inflection points are located , the corresponding frequencies are identified. Resonant frequency and Q factor are then calculated from the measured inflection point frequencies (3.9) & (3.10).

The primary advantage of the system is that it is independant of the resonator transmission coefficient(frequency characteristic) at the resonant frequency as well as the 3-dB or inflection points .In this system , the inflection

points are obtained , as mentioned , by mathematical evaluation , and are thus not affected by instabilities in the detector such as :

- Deviations of the detector characterstic from the square-law ,

- Temperature instabilities of the detector. (Typically , 0.015db/° C).

- Frequency response of the detector. (Typically , ±0.2 db/octave in 10 MHz to 8 GHz range).

Since the detector output is digitized through the sample-and-hold circuit of the A/D converter , short term instabilities of the detector have little or no effect on the converted signal.

The inflection points on the resonance curve can be evaluated very accurately using numerical techniques and therefore , the resonant frequency and Q factor can also be determined very accurately. In addition , the measurement system is very fast , so that the VCO instabilities may have less effect on the computed resonant frequency and Q factor. (When the measurement process is slow VCO instabilities cause frequency drift during the measurements , resulting in errors). Higher measurement speed means that the system responds faster to changes in the resonant frequency and Q factor , which can be used to monitor changes in the related parameters such as dieletric constant and loss factor.

Evaluation of the Q factor from the inflection point frequencies eliminates the necessity of making precise measurements at the 3-dB points on the resonance curve thus making this method eminently suitable for measurement of high values of Q factor , since the resulting sharp changes in the first or second derivative are easily detected.

The system is completely automated and thereby avoids human error and fatigue during the measurement process , in addition to making mesurements faster. Manual measurement of the resonant frequency and the 3-dB frequencies requires careful and often tedious search for these points with the resulting possibility of introducing errors.

Since the processing of the data and the evaluation of the resonator parameters are all done by a computer, the transfer of the data and results between different systems is possible. Thus , for example , using the IEEE 488 bus , data acquired by bus compatible instruments can be transferred to the computer so as to utilize the readily available signal processing software.

3.2.1 Numerical Processing Techniques.

The main task to be performed by the computer is the determination of the frequencies corresponding to the inflection points. This is accomplished by determining the inflection points from the sampled data and identifying the

corresponding frequencies.The inflection points on the curve may be identified by two general methods viz.:

-Obtaining the positive and negative maxima of the first derivative and the corresponding frequencies.

-Obtaining the points at which the second derivative of the resonance curve is zero and identifying the corresponding frequencies.

The sampled data gathered from the experimental system may contain inherent errors due to noise ;these errors are not usually predictable and are distributed according to some statistical pattern.Interpolating this data and differentiating the resulting interpolation function would cause errors in the derivatives as well.The sampled data must therefore be 'smoothed' before being used , to remove as many of the statistical errors as possible. Thus the inflection points can be determined by :

1. Smoothing the input data by linear interpolation , and
2. Differentiating the smoothed data to obtain the first derivative.

3.2.1.1 Smoothing The Input Data.

Suppose that a set of sampled data points $y_1, y_2 \ldots . y_n$ is obtained at frequencies $x_1, x_2 \ldots . x_n$ .Then the smoothing function provides a vector $z = [z_1, z_2 \ldots . z_n]$ where except

for the end points x_1 and x_n , each value z_i is obtained by evaluating at x_i the least squares polynomial of degree 1 relevant to the 3 successive points (x_{i-1}, y_{i-1}) , (x_i, y_i) and (x_{i+1}, y_{i+1}) [17].

3.2.1.2 Differentiating The Smoothed Data.

Once the data has been smoothed , numerical differentiation algorithms are applied to it.These algorithms provide a vector of first derivatives $z=[z_1, z_2 \ldots z_n]$ given a set of smoothed data points $y=[y_1, y_2 \ldots y_n]$ at the frequencies $x=[x_1, x_2 \ldots x_n]$.Except for the end points x_1 and x_n , z_i is the derivative of the Lagrangian interpolation polynomial of degree 2 relevant to the 3 successive points (x_{i-1}, y_{i-1}) , (x_i, y_i) and (x_{i+1}, y_{i+1}) .

If the data is obtained at equally spaced points , other algorithms can be used to compute a vector of first derivatives , where each point except x_1, x_2 and x_{n-1}, x_n are obtained from the Lagrangian interpolation polynomial of degree 4 relevant to the 5 successive points (x_{i+k}, y_{i+k}) , $k=-2,-1,\ldots 2$.

If the spacing ' h ' between samples is made small , then the interpolation polynomial f(x) is essentially a straight line over the 3 or 5 sampled points so that the above algoritms are applicable here.Also , since the linearity of the resonance curve is also the greatest at the inflection

points [3] its correspondence to f(x) is also the best around the inflection points, so that the above algorithms give the best results around the inflection points.

3.3 UNCERTAINITY ANALYSIS.

In the following analysis, the detector effects are assumed negligible. This is because the detector characteristic can be considered to be piece-wise linear, with a specified constant sensitivity over a given range of input power. Especially at high values of the Q factor, the tuning bandwidth is small so that power level variations of the VCO (over the tuning bandwidth) are also small. Also, as long as the detector input power does not exceed the range of square-law operation, the output voltage of the detector can be assumed to be a function of the input power only.

The uncertainity of a measured experimental quantity can be estimated on the basis of the uncertainities of the primary measurements. Thus, if a given function $R = R(x_1, x_2, \ldots x_n)$ and w_R is the uncertainity of R while $w_1, w_2, \ldots w_n$ are the uncertainities of $x_1, x_2, \ldots x_n$, the uncertainity w_R of the function R can be expressed in terms of the uncertainity $w_1, w_2, \ldots w_n$. If the uncertainities $w_1, w_2, \ldots w_n$ are given with the same odds, the uncertainity w_R will be specified with these odds. Thus [23],

$$w_R = \left(\left(\frac{\partial R}{\partial x_1} \cdot w_1 \right)^2 + \left(\frac{\partial R}{\partial x_2} \cdot w_2 \right)^2 + \cdots \left(\frac{\partial R}{\partial x_n} \cdot w_n \right)^2 \right)^{1/2}$$

Using the above relation , the uncertainity of the Q factor can be expressed in terms of the uncertainity of the inflection point frequencies f_1 and f_2. This would however require prior knowledge of the true (or the closest approximate) values of the inflection point frequencies. In order to make a more generalized uncertainity analysis , the theoretical maximum uncertainity will be evaluated instead using a knowledge of only the resonant frequency and the Q factor of a resonator. Two components contribute to the absolute uncertainity in frequency Δf:

-the counter uncertainity Δc , and

-the uncertainity resulting from the algorithm used to determine the inflection point Δf_A.

Δf_A includes :

- the absolute uncertainity in VCO frequency Δf_{VCO}
- the effect of intersample spacing P [V]
- the effect of A/D converter quantization error q [V] .

Let the slope of the VCO characteristic be S [Hz/V]. From Figure 5 it is evident that since the system evaluates the first derivative of the voltages obtained , the actual voltage measured is

$$V = \Delta V \pm q \text{ [V]}.$$

The absolute uncertainity due to intersample spacing Δf_R = SP [Hz].

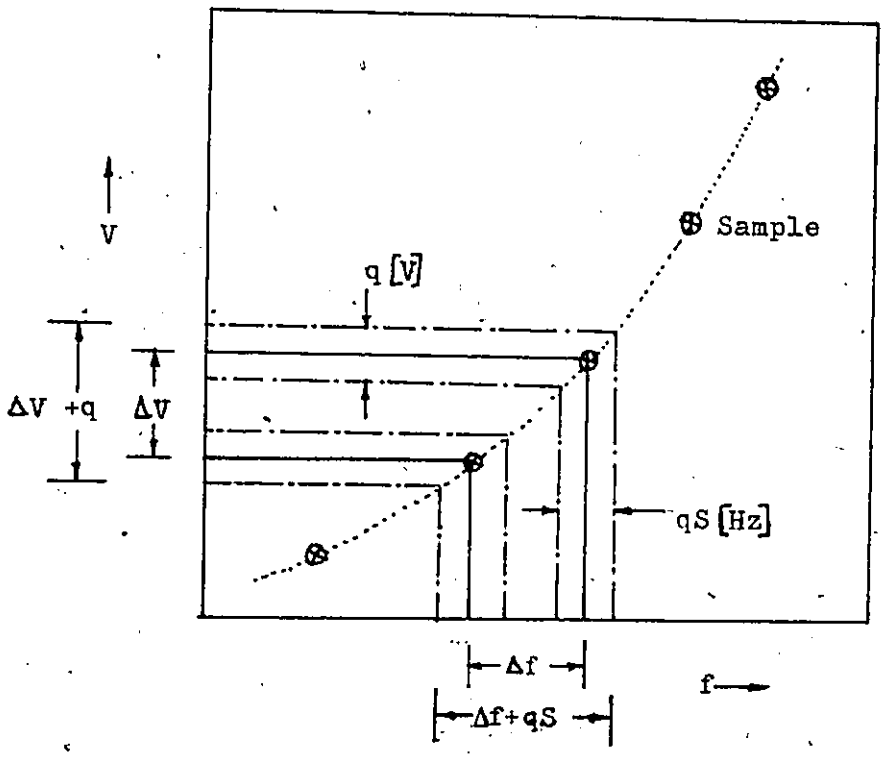

Figure 5: Effects of A/D converter quantization error q on the intersample frequency spacing.

Therefore , from Figure 5 the actual increment in frequency , taking into account the effect of the A/D converter quantization error is

$$f = \Delta f_R + q.S \ [Hz].$$

The maximum uncertainity in frequency is then

$$\Delta f = (\Delta f_R + q.S) + \Delta f_{VCO} + \Delta c \qquad (3.11)$$

The resonant frequency is $f_0 = (f_1 + f_2)/2$, where f_1 and f_2 are the inflection point frequencies. Thus , the absolute uncertainity in f_0 is $\Delta f_0 = \Delta f_1 + \Delta f_2$, where Δf_1 and Δf_2 are the absolute uncertainities in determining f_1 and f_2 respectively.

Assuming $\Delta f_1 = \Delta f_2 = \Delta f$, therefore , the absolute uncertainity in measured resonant frequency is :

$$\Delta f_0 / f_0 = 2 \Delta f / f_0 \qquad (3.12)$$

Also , using (3.10) ,

$$\Delta Q_L / Q_L = 2 \Delta f (1+\sqrt{3} Q_L) / f_0 \qquad (3.13)$$

3.3.1 Uncertainity Case Study.

In this case study , the above analysis is used to derive the system specifications using realistic parameters.

Let the resonant frequency $f_0 = 1$ GHz ,

-the D/A converter resolution R =2.44 mV , (12-bit converter with f.s. range of ± 5 V),

-the A/D converter quantization error q = 1.22 mV , (for a 12-bit converter with a f.s. range of ± 5 V),

-the uncertainity in the counter reading $\Delta c/c = 10^{-6}$, so that Δc=1 kHz.

- Δf_{VCO} =20 kHz and the slope S = 1 MHz.

Now , $\Delta f_R = R.S$ [Hz]

and $\Delta f = (\Delta f_R + q.S) + \Delta f_{VCO} + \Delta c$ [Hz]

$= 10^{6} \times (3.66) \times 10^{-3} + 10^{3} + 20 \times 10^{3}$

=24.66 kHz.

Therefore $\Delta f_o = 2(\Delta f)$ =49.32 kHz.

$$\therefore \frac{\Delta f_o}{f_o} \simeq 50 \text{ ppm}$$

Also , from (3.13) , for Q_L = 1000 ,

$$\frac{\Delta \theta_L}{\theta_L} = 8.66 \%$$

Thus , the theoretical maximum uncertainity in resonant frequency is 50 ppm while that of the Q factor is 8.66 % for a Q of 1000.It is seen from (3.13) that the uncertainity of the Q factor is a function of the resonant frequency and the Q factor;the uncertainity of the measured Q factor will therefore increase with higher values of the Q factor.

The above values of the uncertainities of f_o and Q factor are used in evaluating the performance of the measurement system.

Chapter IV

SYSTEM DESCRIPTION.

4.1 INTRODUCTION

This chapter provides a description of the experimental system and is divided into two sections :

1. Data acquisition
2. Data processing

The description is further sectioned into two areas : hardware and software. The hardware describes the equipment and components used , while the software deals with algorithm and program development.

4.1.1 Data Acquisition.

Figure 6 shows a block diagram of the experimental system. In the Data Acquisition Phase the resonator response is obtained on a point-by-point basis between any two frequencies (F_A , F_B) .The data is obtained as follows. A starting digital code is applied to the D/A converter and the corresponding analog voltage is fed to the VCO , thus providing an output signal at a frequency F_A. The VCO output signal is applied to the resonator and the resulting resonator output

as well as the input are detected and introduced into the computer via the A/D converter channels. The VCO frequency, as measured by the counter, is also fed into the computer through the Digital I/O lines.

The transmission loss $T(\omega)$, which is a ratio of the output to the input power of the resonator, is calculated and stored in an array, along with the corresponding frequency. The next point is obtained by incrementing the digital code thus providing an output signal at a higher frequency, and the transmission loss at this frequency is obtained and stored along with the corresponding frequency as before.

This procedure is carried out over the complete range of frequencies from F_A to F_B. At the end of this data acquisition phase, the transmission loss and the corresponding frequency at each frequency between F_A and F_B are obtained and stored in the computer memory.

Any change occurring in the input data is thus recorded immediately within the survival time of the data. This data is then processed at a slower rate. The calculated values of f_0 and Q factor are available at the end of the data processing stage. Changes in f_0 and Q factor (in repeated measurements) indicate changes in the input data samples and hence in the process being monitored. The data processing phase is seperated from the data acquisition phase in order

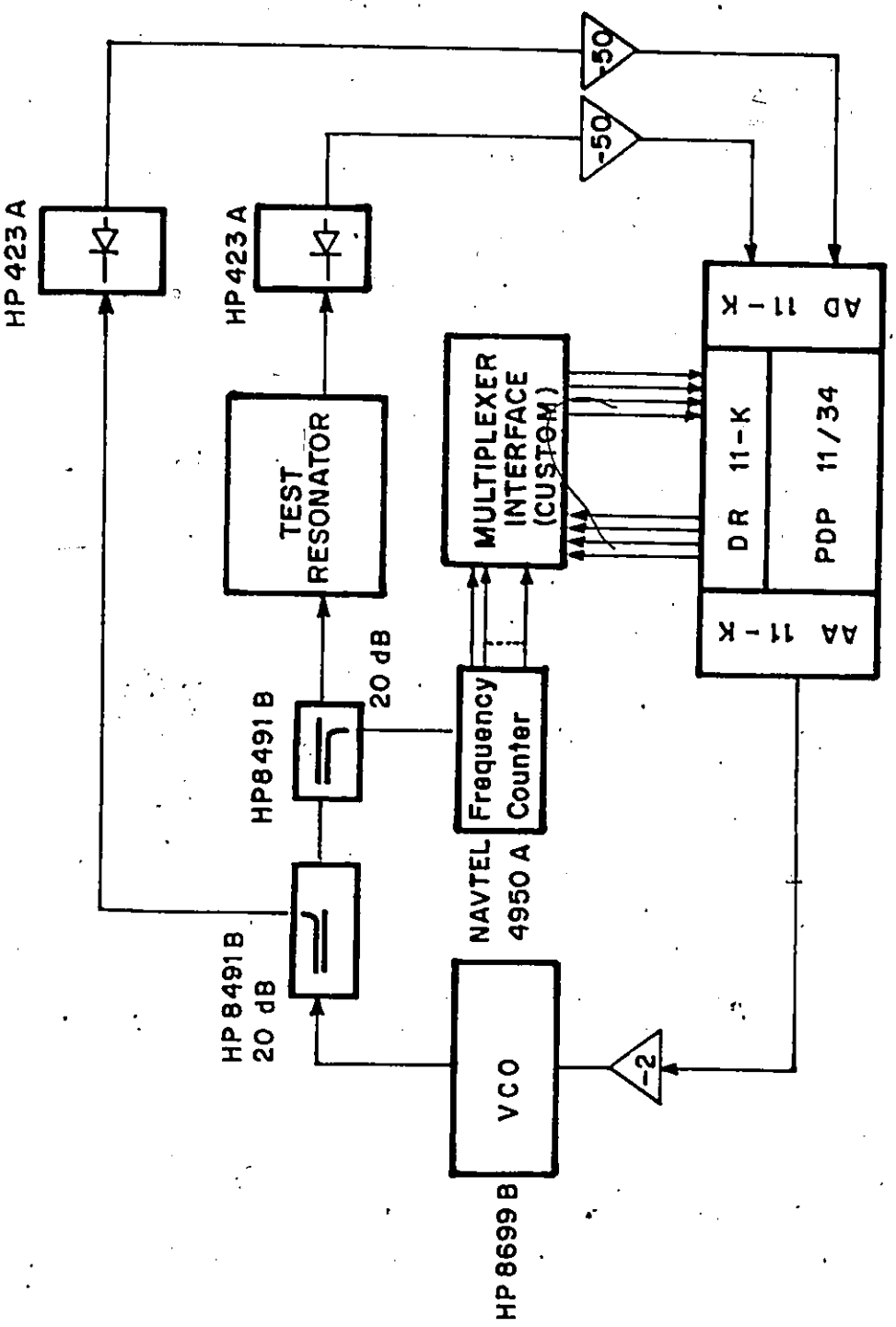

Fig. 6: Experimental Arrangement.

to permit the system to capture any changes in the input data in real-time , so that the slower execution times of the mathematical routines do not degrade the system speed.

4.1.2 Data Processing.

Once the data have been acquired , numerical techniques are used to identify the inflection points.As mentioned earlier , smoothing techniques are applied to the data to obtain the least squares fit of degree one .The smoothed data is then differentiated.

Once the derivative at each point is known , the maximum positive and negative derivatives and their corresponding frequencies are identified. These are the inflection points.The Q factor and f_o are calculated from the inflection points and the results printed.

4.1.3 System Control.

The data acquisition and processing as well as the print-out of the results are carried out under computer control, through the K-Series Laboratory Peripheral routines of the PDP 11/34 computer. A command file is used to run the experiment continuously , providing a printed output of the resonant frequency and Q factor at the end of each measurement so that the resonator can be monitored continuously for changes in its characteristics. The programs and subroutines used are discussed in the software section.

4.2 HARDWARE.

The equipment used in the system includes a PDP 11/34 computer, a HP 8699B oscillator , a NAVTEL 4950A frequency counter , 423A crystal detectors , D/A converters and assorted signal conditioning amplifiers for the D/A converters and A/D Converters.A brief description of each of these elements is provided here.

4.2.1 The PDP 11/34.

A PDP 11/34 minicomputer using the RSX-11M real-time multiuser operating system is utilized for data acquisition , data processing and overall system control through the K-Series Peripheral Drivers.The computer system consists of a KD11-EA central processor communicating with the KY11-LA console unit , the core/MOS memory unit and various peripheral devices through a Unibus [26].

4.2.2 The Oscillator.

The Model HP 8699B oscillator is an electronically tuned signal source covering the frequency range from 0.1 to 4.0 GHz in two bands (0.1 to 2 GHz and 2 to 4 GHz). It consists of a solid-state oscillator that uses a hybrid micro-circuit YIG-tuned oscillator and mixer , an integrated circuit amplifier , and a PIN modulator-attenuator [21].

4.2.3 The Counter.

The NAVTEL 4950A frequency counter covers the frequacy range from 80 MHz to 1.25 GHz . It has an 8-digit LED display with automatic decimal point positioning. Display resolution is front-panel selectable at 1 kHz , 100 Hz , 10 Hz , 1 Hz and 0.1 Hz. Measurement unit indicators (MHz , kHz or Hz) and an overflow indicator are provided. All displayed measurement data is also available in a CMOS compatible , parallel BCD output on a rear panel connector [20].

4.2.4 Multiplexer Interface.

Figure 7 shows the multiplexer interface used to transfer the BCD output correponding to the displayed measurement data from the counter to the computer via the DR 11-K lines. In the figure , Dk1 - Dk8 are the BCD outputs from digit k , k=1,2,...8. The DOUT line 3 is used to provide the strobe pulse , while the DOUT lines 0 - 2 are connected to the select lines of the multiplexers.

One diplayed digit is read at a time onto the DINP bus , and the frequency is calculated using :

$$\text{Frequency} = \text{Digit } 0(0.001) + \text{Digit } 1(0.01) + \text{Digit } 2(0.1) + \text{Digit } 3 + \text{Digit } 4(10) + \text{Digit } 5(100) + \text{Digit } 6(1000) \qquad (4.1)$$

The decimal point in the displayed frequency is fixed through the front panel resolution selector . Once this is fixed , the digits read in through the DINP lines are

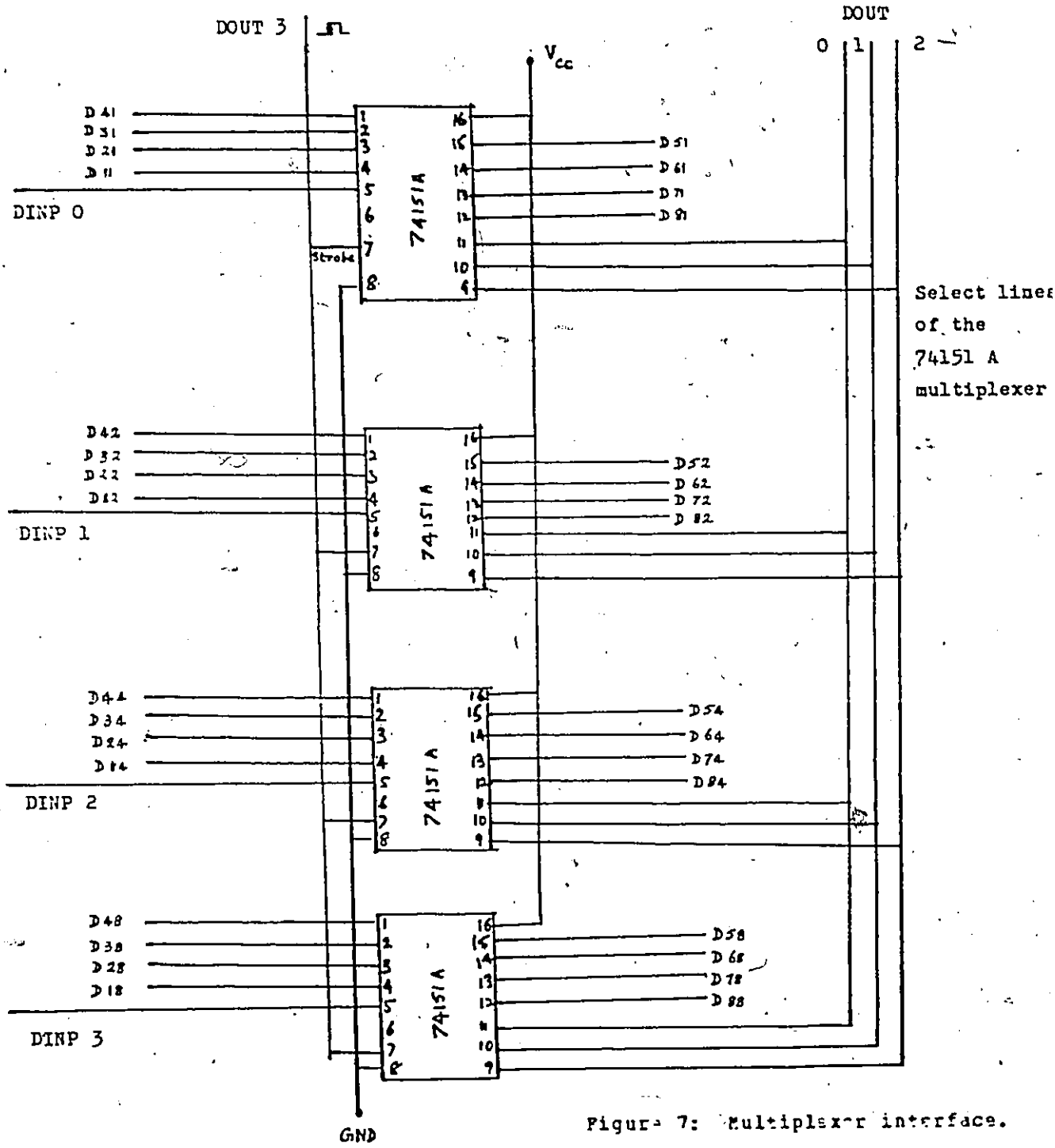

Figure 7: Multiplexer interface.

'weighted' appropriately to yield the displayed frequency as in eqn.(4.1).

4.2.5 Theoretical System Specifications.

In the Uncertainity Case Study of Section (3.3), the A/D converter and D/A converter specifications were presented. In this section these specifications will be used to determine the range of Q factors that the system can measure within specified uncertainities. In order to do this, it must first be ensured that the A/D converters are able to detect the smallest change in detector output occurring due to an increment in the frequency. This is done by estimating the smallest change in this output voltage that can occur over a specified range of resonant frequencies and Q factors. This estimation is carried out in the following way.

In section 3.3, the normalized transmission loss was obtained as

$$\frac{T(f)}{T(f_0)} = \frac{1}{\left(1 + 4Q_L^2 (\delta f/f_0)^2\right)} \qquad -(4.2)$$

and the condition at the inflection point as

$$\frac{2Q_L(f-f_0)}{f_0} = \pm \frac{1}{\sqrt{3}} \qquad (4.3)$$

where equations (3.7) and (3.8) have been renamed for convenience as (4.2) and (4.3) respectively. Obtaining $T'(f)$ from (4.2) and substituting (4.3) in it gives,

$$T'(f) = \pm \frac{36}{16\sqrt{3}} T(f_0) \frac{Q_L}{f_0} \qquad (4.4)$$

-at the inflection points.

From $$T(f_0) = \frac{4\beta_1\beta_2}{(1+\beta_1+\beta_2)^2}$$

with critical coupling, $\beta_1 = \beta_2 = 1$. Therefore, $T(f_0) = 4/9$. Substituting this in (4.4)

$$T'(f) = \pm \frac{\sqrt{3}}{3} \frac{Q_L}{f_0} \qquad (4.5)$$

-at the inflection points. Equation (4.5) gives the maximum slope of the curve, $T'(f)$, at the inflection point. Consider the operation of the system in a 1 GHz to 2 GHz range.

The maximum slope dT/df occurs when $f_0 = 1$ GHz.

$$\text{Max } T'(f) = \pm Q_L \frac{\sqrt{3}}{3} \times 10^{-9} \quad [\text{Hz}] \qquad (4.6)$$

From the Uncertainity Case Study, the absolute uncertainity in measured frequency = 24.66 kHz, the slope of the VCO tuning characteristic is 1 MHz/V, and the A/D converters as well as the D/A converters have 12 bit resolution and a f.s. range of ±5 V.

$$\left.\frac{dT}{df}\right|_{\text{inflection}} = \pm \frac{\sqrt{3}}{3} Q_L \times 10^{-9} \quad \text{from (4.6)}$$

$$\Delta T(f) \simeq \Delta f \cdot \left.dT/df\right|_{\text{inflection}}$$

Since $\Delta f \simeq 25$ kHz, therefore $\Delta T(f) = 25(\sqrt{3}/3)\, Q_L \times 10^{-9}$ (4.7)

Now, $T(f) = \frac{\text{Detector voltage at cavity output}}{\text{Detector voltage at cavity input}} = \frac{V_o(f)}{V_{in}(f)}$.

Therefore,

$$\Delta T(f) = \frac{\Delta V_o(f)}{V_{in}(f)} \qquad (4.8)$$

$V_{in}(f)$ is the detected voltage at the cavity input. This voltage is proportional to the power at the input of the cavity. $V_{in}(f)$ is measured experimentally as $\simeq 0.16$ V. from (4.7) and (4.8),

$$\Delta V_0(f) = \frac{25\sqrt{3}}{3} Q_L \times 10^{-9} \times V_{in}(f) \quad [V]$$

$$= 2.17\, Q_L \times 10^{-6} \quad [V] \qquad (4.9)$$

Equation (4.9) represents the change in the output signal corresponding to a single frequency increment.

The maximum output voltage $V_0(f)_{max}$ occurs at resonance : $T(f_0) \times V_{in}(f) = \frac{4}{9} \times 0.16 = 0.07$ V

(assuming critical coupling so that $\beta_1 = \beta_2 = 1$).

Table 3 evaluates the ratio $\Delta V_0(f) / V_0(f)_{max}$ for various Q_L for the above experimental system. The values obtained for $\Delta V_0(f)$ and $V_0(f)_{max}$ change depending on the attenuation introduced into the system (to prevent reflections). The A/D converter specifications must be defined for a particular ratio of $\frac{\Delta V_0(f)}{V_0(f)_{max}}$, corresponding to a particular configuration.

In the case of the above system, if 12-bit A/D converters were being used, the quantization error with a ±5 V f.s. range is 1.22mV. Therefore the ratio of :

$$\frac{\text{quantization error}}{\text{maximum voltage}} = \frac{q}{V_{max}} = \frac{1.22 \times 10^{-3}}{10} = -78.3 \text{ dB.}$$

TABLE 3

Theoretical system specifications.

Ratios of the smallest change in output voltage ($\Delta V_0(f)$) to the maximum output voltage ($V_0(f)_{max}$) for various Q factors.

Q	$\Delta V_0(f)$ (v)	$\frac{\Delta V_0(f)}{V_0(f)_{max.}}$	$\frac{\Delta V_0(f)}{V_0(f)_{max.}}$ (dB)
10	2.17×10^{-5}	3.1×10^{-4}	-70
100	2.17×10^{-4}	3.1×10^{-3}	-50
500	1.085×10^{-3}	1.55×10^{-2}	-36
1000	2.17×10^{-3}	3.1×10^{-2}	-30
10,000	2.17×10^{-2}	0.31	-10

From an inspection of Table 3 , it is seen that the ratio of $\Delta V_o(f)/V_o(f)_{max}$ is =70 dB for a Q of 10 , while the ratio of q/V_{max} for the A/D converter is -78 dB.Thus 12-bit converters can be used to measure a Q > 10. Table 3 , thus has the dual purposes of :

1. Specifying the A/D converter resolution required in order to measure a given Q factor , and
2. Specifying the minimum noise /signal level in the system.

The second point follows , since if the noise/signal level is not smaller than the ratio of $\Delta V_o(f)/V_o(f)_{max}$ then the change $\Delta V_o(f)$ in the signal outputs will not be detected. This is especially important in the case of low Q resonators , where the signal change $\Delta V_o(f)$ is small (between adjacent samples).This implies that in such cases , the noise/signal levels must be smaller than $\Delta V_o(f)/V_o(f)_{max}$. For the above hardware specifications , therefore, the smallest Q factor that can be measured by the system is =10 , with an uncertainity of 0.08% , when uncertainity of f_o is 50 ppm. From the uncertainity analysis of section 3.3 , the theoretical measurement uncertainities were found to be 50 ppm in frequency and 0.66% in Q for a Q factor of 1000.

The smallest Q factor that can be measured by the system with an uncertainity of 0.08% is 10.The uncertainity in f_o is 50 ppm. Also , the measurement uncertainity increases with Q factor so that a Q factor of 1000 is measured with an uncertainity of 8.86%.

4.3 SOFTWARE

This section describes the algorithms used and the computer program development. It is divided into three sections::

1. Smoothing and Differentiation of Sampled Data.
2. K-Series Peripheral Routines.
3. System integration.

4.3.1 Smoothing and Differentiation of the Sampled Data.

As described in earlier sections , the data samples are smoothed using linear least squares interpolation techniques before differentiation. Once the derivatives are known the peak positive and negative values of the derivatives are identified as the inflection points.Since the features of interest are the points at which the slope maxima occur , the actual magnitudes of the derivatives are not as important as the relative values of the derivatives at the different points. Thus , as long as the truncation and round-off

errors are not large enough to make the calculated values of the first derivatives completely wrong , they can be tolerated. In the following sections the truncation errors for the 3-point and 5-point formulas are calculated , to determine whether the errors are small enough to allow the use of these formulas .

The truncation error for the Lagrangian interpolation formula corresponding to the 3 points (x_{i-1}, y_{i-1}), (x_i, y_i) and (x_{i+1}, y_{i+1}) is [17] :

$$e_{t3} \simeq \frac{1}{6} \frac{x_i - x_{i-1}}{x_i - x_{i+1}} y'''(\xi_i) \qquad i = 2, 3, \ldots n-1$$
$$x_{i-1} \le \xi_i \le x_{i+1}$$

For the 5 point Lagrangian interpolation formula using equally spaced points (x_{i+k}, y_{i+k}) , $k=-2,-1,\ldots 2$,

$$e_{t5} \simeq \frac{24}{5} h^2 y^5(\xi_i) \quad \text{where } h = x_i - x_{i-1}$$
$$x_0 - 2h \le \xi_i \le x_0 + 2h$$

Assuming h=25 kHz (the minimum allowable frequency step) and estimating $y'''(\xi_i)$ and $y^5(\xi_i)$ at the inflection points on the curve where $2Q_L(f-f_0)/f_0 = \pm 1/\sqrt{3}$,

$$e_{t3} \simeq 2.92 \times 10^{-6} \quad [Hz^{-1}]$$
$$e_{t5} \simeq 6.89 \times 10^{-9} \quad [Hz^{-1}]$$

The peak positive and negative magnitudes of the first derivatives (corresponding to the inflection points) are on the order of 10^{-3} $[Hz^{-1}]$. Thus , the above truncation errors are acceptable and the above 3-point as well as 5-point formulas can be used here.

4.3.2 K-Series Laboratory Peripheral Routines.

Laboratory peripheral modules (K-Series) are supported on the PDP 11/34 through a set of program-callable routines that are linked with the user's task during task building [22]. The peripheral modules used here are the DR 11-K digital I/O interface, the AD 11-K A/D converter and the AA 11-K D/A converter.

4.3.3 AD 11-K A/D converter.

The AD 11-K is a 12 bit successive approximation converter that enables the user to sample analog data at specified rates and to store the equivalent digital value for subsequent processing. Sixteen A/D converter channels are available on this module with ±5 v input range and 12-bit resolution. Sample-and-hold circuitry is available at the input to the converter.

The A/D converter channels are used here to enter the voltages corresponding to the resonant cavity input and output powers to the computer.

4.3.4 AA 11-K D/A Converter.

The AA 11-K module includes four 12-bit D/A converters and an associated display control. The input range of the converters is ±5 V.

Channel zero of this module is used to output the analog tuning voltage to the VCC , at each sample point.

4.3.5 DR 11-K Digital I/O Interface.

This is a general purpose digital I/O interface capable of the parallel transfer of upto 16 bits of data under program control between the PDP 11 UNIBUS and an external device.

The K-Series peripheral support routines are used for the following processes :

1. digital input
2. digital output
3. single A/D input.
4. single D/A output.

4.3.6 Program use of K-Series Routines.

The K-Series support routines are linked to the main program at taskbuild time. The format for these routines are given here in FORTRAN , but they can be accessed by MACRO-11 programmers using subroutine linkage programs or through other special purpose macros. Table 4 shows the FORTRAN subroutines for the K-Series laboratory peripherals used here.

TABLE 4

K-Series peripheral routines used

Subroutine	Function
ADINP	Initiates a single analog input.
DAOUTO	Initiates a single analog output.
DINP	Initiates a digital input.
DOUT	Initiates a digital output.

4.3.7 ADINP.

The ADINP routine obtains a single word as input from the A/D converter. It is invoked as follows:

CALL ADINP ([iflag],[ichan],ival)

iflag specifies the gain options in the input signal and is usable only with the AM 11-K multiple gain multiplexer option not available here.

ichan specifies the channel to be sampled.

ival recieves the sample.

4.3.8 DAOUT0

This routine outputs a single word through D/A converter channel zero. It is invoked using :

CALL DAOUT0(IX)

IX : specifies the input word to be converted.

4.3.9 DOUT.

This routine outputs a single 16-bit word through the DR 11-K interface. Only the bits specified in a mask are altered.

This routine is invoked as follows:

CALL DOUT ([iunit],[mask],IOSB,idata)

iunit is the DR 11-K unit number(default is zero)

mask indicates the bits that can be altered (177777 indicates that all bits can be altered).

IOSB is a 2-word I/O status array specifying the status of the call and the buffer size in words.

idata is the 16-bit output word that is sent to the DR 11-K.

A faster version is available and is invoked as a subroutine:

iout=IDOUT(0,,,IDATA)

where iout recieves a copy of the data transferred.

The DOUT routine is used to provide the digital code to lines 0 to 3 which are needed by the DINP interface circuitry during execution of a DINP routine.

4.3.10 DINP.

This routine inputs a 16-bit word from the DR 11-K interface . It can be invoked as follows:

CALL DINP ([iunit],[mask],IOSB,input)

iunit is the DR 11-K unit number (default is 0)

mask indicates which of the bits in the input buffer are to be cleared (default is 177777)

IOSB is a two word I/O status block array specifying the status of the call and the buffer size in words.

input recieves the data from the DR 11-K .

A faster version is available and is invoked as a subroutine:

input=IDINP(0,,,,)

where input is as above. On the completion of the DINP routine the contents of the information on the external device(the counter in this case) is transferred to the UNIBUS of the computer.

4.3.11 System Integration.

Figure 8 shows the integrated flowchart of the system.The flowchart is self-explanatory.

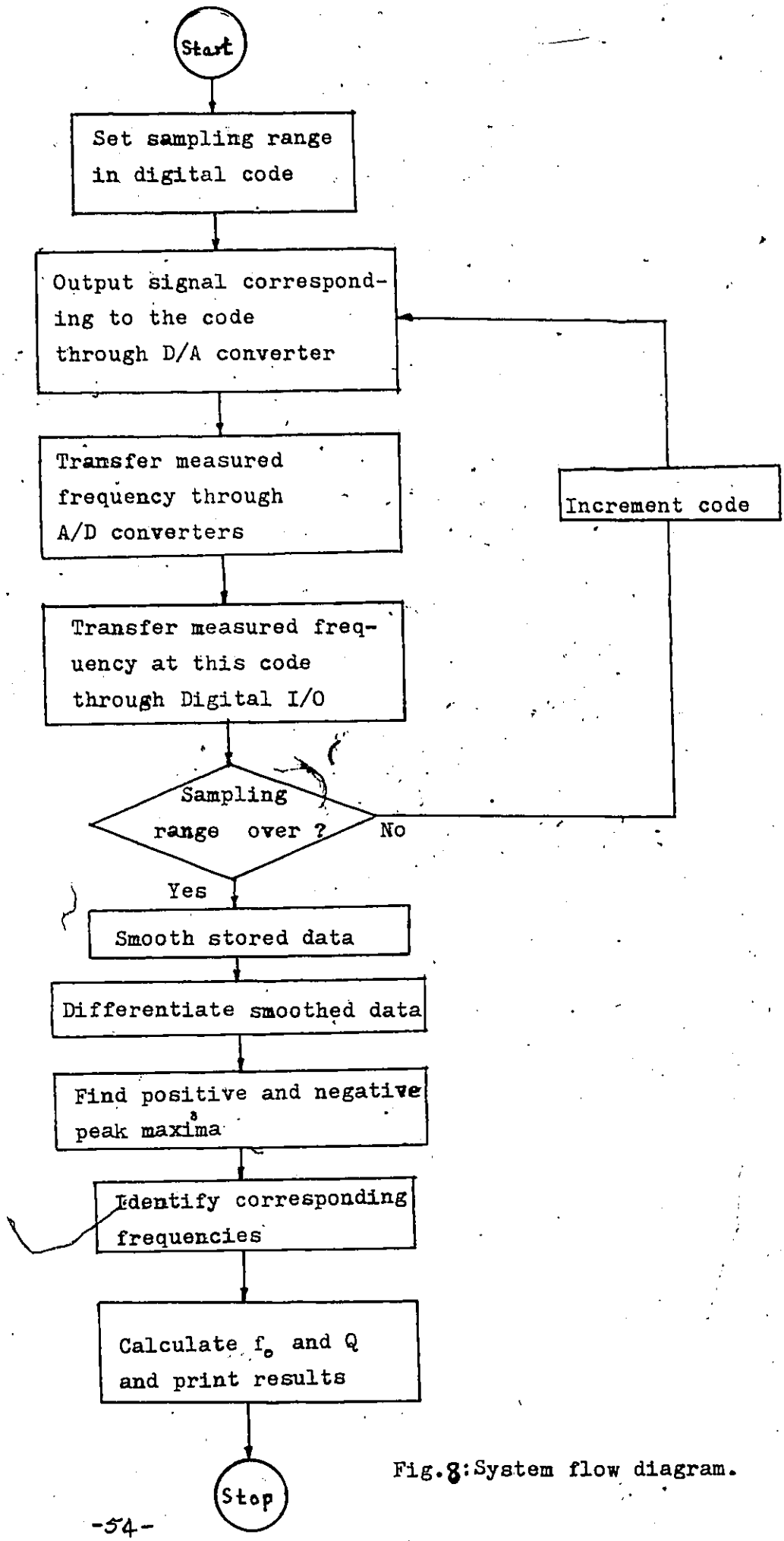

Fig.8: System flow diagram.

Chapter V

SYSTEM SIMULATION.

Simulation performs a very useful role in the development of new measurement systems. It provides a means by which various design concepts can be used to evaluate the performance of a given system, prior to its fabrication. The information and data obtained by simulation have real world applications. Simulation provides information not only about the system's potential, but also about its limitations. In this way a fuller understanding of the potential problems of the experimental system can be obtained.

Simulation involves selection of a mathematical model of the experimental system. This model is then used in the simulation process to :

1. Predict system performance under specified operational conditions
2. Test and evaluate the system or its subsystems
3. Identify those parts of the system that require further investigation [24].

In a simulation it is relatively easy to study the effects of changes in one or more of the system parameters.

This is usually more difficult in an actual experimental arrangement. Also , it is often difficult to study the experimental results and to try to determine which factors contributed to the achieved experimental results.For example , in a measurement system such as the present one , these factors could be noise , VCO frequency uncertainity , drift in frequency , resolution of the A/D and D/A converters or errors in the differentiation algorithm.

In a simulation , it is relatively easy to change various parameters individually or simultaneously , and to study the effects of these changes on the system.No previous knowledge of the effects of these changes is required. Simulation is thus used essentially to explore the effects of these changes.

Simulation allows a wider variety of parameter changes than can be obtained in the physical system.In addition , if there are reasons to believe that one or more particular causes are responsible for the achieved experimental accuracy , the effects of these causes can be verified by simulation;this helps in eliminating various causes as possible sources of experimental error. Figure 9 shows the functional block diagram of the mathematical model used in the simulation.The basic features of the various component blocks are defined and integrated into a system;the algorithm simulates the performance of the component blocks.The following

sections provide a description of the noise generation algorithm used in the simulation and the various component blocks of the mathematical model.

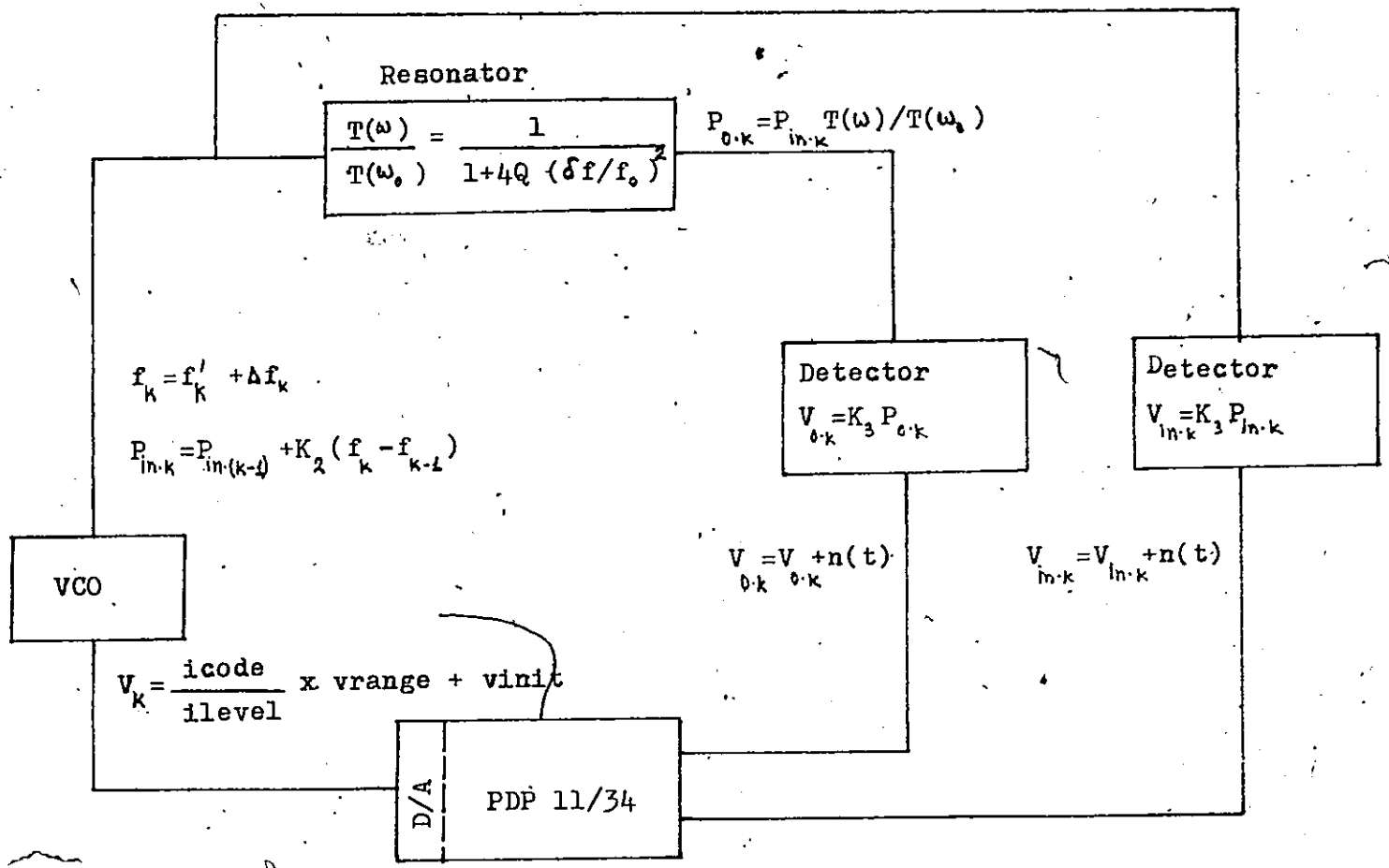

Fig.9: Simulation: Functional block diagram of the mathematical model.

5.0.12 The Pseudo-Random Noise Generator.

Fundamental to the simulation process of a measurement system is the simulation of noise.This section describes an algorithm which simulates the noise in the system. The noise components considered are the Gaussian noise and the power line noise.In the experimental setup this would be sampled by the A/D converters along with the detector outputs.The power line noise level converted will depend on the noise level at the instant of sampling.In the simulation process the instant 'T' at which the noise is sampled is selected randomly , so that the noise level selected for conversion is random.

The noise is simulated using the pseudo-random number generator routine , the .RAN(IL,I2).This routine provides a random number between 0 and 1. The numbers so obtained are then weighted appropriately to obtain the required signal to noise levels.

According to the Central Limit Theorem [18] , the probability density function of the sum ($f_{\bar{X}}(x)$) of a set of random variables $x_1, x_2, \ldots x_n$ with respective densities $f_i(x)$ tends to a normal curve regardless of the shape of the $f_i(x)$.

Thus , if $X = X_1 + X_2 + \ldots\ldots + X_n$

$$f(x) = f_1(x) * f_2(x) * \ldots\ldots f_n(x)$$

Then , $f(x) = \frac{1}{\sigma\sqrt{2\pi}} e^{-(x-\eta)^2/2\sigma^2}$

where η is the mean and σ^2 the variance of the resulting random variable and $\eta = \eta_1 + \eta_2 + \cdots + \eta_n$; $\sigma^2 = \sigma_1^2 + \sigma_2^2 + \cdots + \sigma_n^2$

If X is scaled down by a factor $1/\sqrt{n}$, then the above becomes an equality as $n \to \infty$ provided that :

(1) $\sigma_1^2 + \sigma_2^2 + \cdots + \sigma_n^2 \to \infty$

(2) For some $\alpha > 2$, $\int_{-\infty}^{\infty} x^{\alpha} f_i(x)\, dx < C$ = Constant.

Condition (1) is satisfied if ~~$\sigma_i \to c_1 \to 0$~~ and this is the case for given random variables having equal variances.

Condition (2) is satisfied if all denstities $f_i(x)$ are zero for $|x| > c_2$ [18].

The resulting random variable $x = 1/\sqrt{n}\,(X_1 + X_2 + \cdots . X_n)$ has a Gaussian density function. This random variable is scaled appropriately and used as the Gaussian noise voltage at the detector output , to select the instant 'T' at which the power line noise is sampled by the A/D converters and to simulate the VCO drift and non-linearity effects as explained later.

5.0.13 The VCO.

The factors which are most important in a VCO simulation are the post-tuning drift , the power output variations over the tuning bandwidth , jitter and non-linearity of the voltage/frequency (V/f) characteristic. The jitter in the V/f characteristic causes the output frequency to be different

for repeated tuning at the same tuning voltage.The output frequency is thus no longer a single-valued function of the tuning voltage.

The VCO was simulated as follows.A linear approximation of the V/f characteristic was obtained as shown in Figure 10 the frequency at each of the sample points was found by extrapolation from a specified tuning voltage and slope of the V/f characteristic.A random frequency is then added to the extrapolated frequency obtained from the linear tuning characteristic of Figure 10. Thus the extrapolated frequency of the k th sample , $f_k' = f_{Start} + K_1 V_k$, $k=1,2,...n$, where f_{Start} is the initial frequency used in the extrapolation (Figure 10) , K_1 is the slope of the V/f characteristic and V_k is the tuning voltage of the k th sample.

In addition , a random frequency Δf_k , is added to f_k' to take into account the effects of tuning non-linearity.Thus the frequency of the k th sample is $f_k = f_k' + \Delta f_k$ .The sample frequency (f_k) is thus dependant on the initial frequency (f_{Start}) as well as the random frequnecy (Δf_k).

The effects of jitter can then be simulated simply by changing the value of f_{Start} in different simulation runs;the sampling frequency f_k corresponding to the same tuning voltage V_k would thus be different in each simulation.

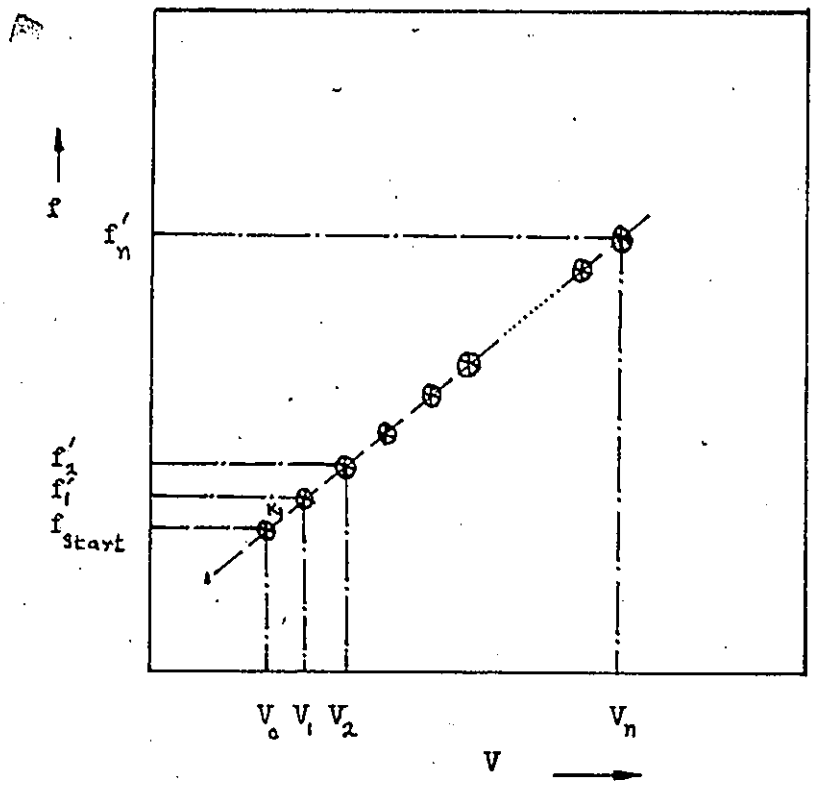

Figure 10: Tuning characteristic of the VCO.

Power level variations of the VCO are simulated in a similar manner using a linear power/frequency (P/f) characteristic. $P_{in\cdot k} = P_{in\cdot(k-1)} + K_2 (f_k - f_{k-1})$, k=1,2,...n , where :

- K_2 is the slope of the P/f characteristic ,
- $P_{in\cdot k}$ is the VCO signal power level for the k th sample

and the initial values $P_{in\cdot 0}$ at f_0 are obtained from the calibration curves of a given VCO.

5.0.14 The Resonator.

The normalized theoretical transmission coefficient of the resonator is :

$$\frac{T(\omega)}{T(\omega_0)} = \frac{1}{\left(1 + 4Q_L^2 \left(\frac{f-f_0}{f_0}\right)^2\right)}$$

The simulated resonance curve is obtained for a given f_0 and Q factor by obtaining the variation of $T(\omega)/T(\omega_0)$ with f , the sample frequency. This ratio is evaluated at each of the sample frequencies.

5.0.15 The Detector and Amplifier .

The transmission coefficient can be expressed as :

$$\frac{T(\omega)}{T(\omega_0)} = \frac{\text{Detector voltage at resonator output}}{\text{Detector voltage at resonator input}}$$

The detector characteristic is assumed to be constant over a specified range of input power. $T(\omega_0)$ is the transmission loss at resonance and is a constant for a given coupling coefficient. Thus the detector action can be simulated by obtaining the detector voltage corresponding to a given input

power with a specified slope of the detector characteristic. A gain factor may be added to indicate amplifier action , although an amplifier with a low noise figure was assumed for simplicity.

In the experimental arrangement , the detector outputs are amplified and introduced to the computer through the A/D converter channels. These signals are affected by noise. Thus the Gaussian noise and the power line noise are added to the detector output levels .

5.0.16 Simulation Flow Diagram.

Figure 11 shows the simulation flow diagram. The simulation was undertaken after a study of the results from initial experiments , as well as the theoretical uncertainity and system specifications. From this study , it was concluded that the main factors that influenced the measurement uncertainity were the VCO effects (frequency jitter , power and frequency drift and non-linearity of the tuning characteristic) and signal/noise levels at the detector outputs. Accordingly , the simulation was used to ,

1. Investigate the effects of the VCO jitter and non-linearity on the measurement accuracy
2. Analyze the effects of various signal/noise ratios on the system.

The mathematical model described in the previous sections was used; the various blocks of the model were interlinked by the simulation algorithm and appropriate parameters were changed to study the effects of jitter or S/N levels on the measurement uncertainities.

As in the experimental arrangement the simulation process was divided into a data acquisition phase and a data processing phase.The following description of the simulation algorithm is thus considered in terms of the two phases of operation.

5.0.16.1 Simulation : Data Acquisition Phase.

The sampling range was fixed in terms of digital code;this range is such as to provide the required tuning bandwidth for a given range of Q factors.The second parameter to be considered was the initial frequency (f_{Start}) , mentioned in the mathematical model (section (5.0.13)). In the study of the VCO jitter , different values were assigned to f_{Start} (for a given tuning voltage).In the study of the effects of various S/N ratios , f_{Start} was fixed at a particular value.

The random number routine was used to obtain the Gaussian noise as well as the sampled value of the power line noise , as described in section 5.0.12. In the study of the effects of S/N ratios , the amplitude of these noise components were altered , thus providing a range of S/N ratios.

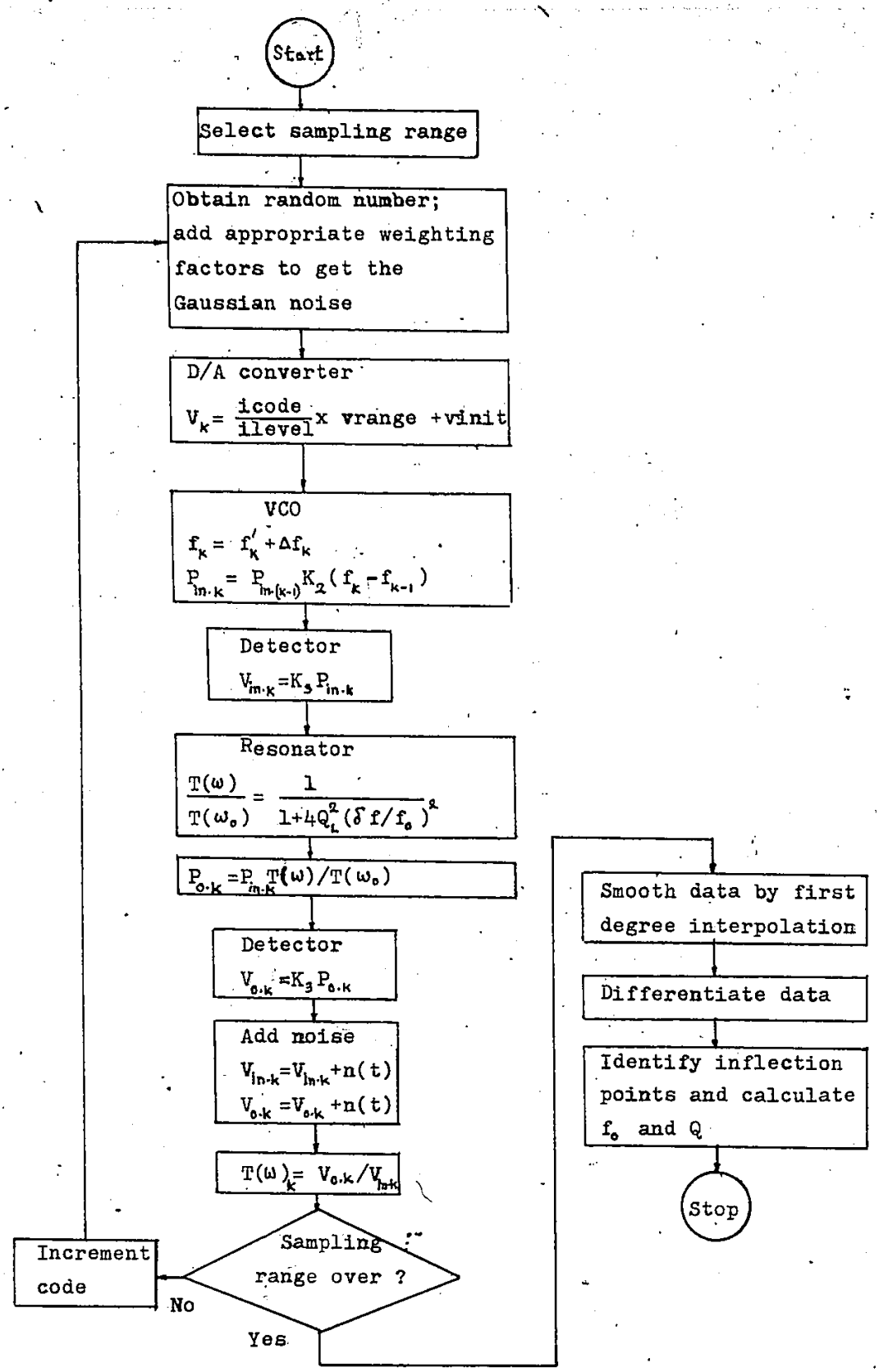

Fig.II: Simulation flow diagram.

The tuning voltage for the VCO (V_k) was provided by the D/A converter and is simulated using :

$$V_k = \frac{\text{icode}}{\text{ilevel}} \times \text{vrange} + \text{vinit}$$

where , icode is the digital code corresponding to a sample , ilevel is the total number of levels available for an n bit D/A converter, vrange is the D/A converter output range , and vinit is the lower limit of this range.

The selected value of V_k was used along with f_{Start} and K_1 (section 5.0.13) to obtain the VCO signal frequency $f_k = f'_k + \Delta f_k$, k=1,2,...n.The VCO signal power level was also obtained as $P_{in\cdot k}=P_{in(k-1)}+K_2 (f_k - f_{k-1})$, k=1,2,...n. In this way , the k th sample point was obtained at a frequency $f_k = f'_k + \Delta f_k$ and a power level $P_{in\cdot k}=P_{in(k-1)}+K_2 (f_k - f_{k-1})$ .This signal was applied to the simulated resonator to obtain the corresponding output power :

$$P_{0\cdot k} = P_{in\cdot k} \frac{T(\omega)}{T(\omega_0)}$$

The detector outputs corresponding to the resonator (input and output) levels were then calculated.The two detectors were assumed to have a constant and equal sensitivity K_3 over the range of input powers used.Thus , $V_{in\cdot k}=K_3 (P_{in\cdot k})$ and $V_{0\cdot k}=K_3 P_{in\cdot k} T(\omega)/T(\omega_0)$ were obtained where : $V_{in\cdot k}$ is the detector output level corresponding to the power level at the resonator input for the k th sample point , and $V_{0\cdot k}$ is output level at the resonator output for the same sample point.

The noise level n(t) was added to $V_{in\cdot k}$ and $V_{o\cdot k}$. In the study of the VCO jitter a fixed level of noise was added to $V_{in\cdot k}$ and $V_{o\cdot k}$; in the study of noise effects various simulation runs were carried out with a different noise level in each case, thereby providing a set of simulation results corresponding to different S/N levels.

The transmission coefficient $T(\omega)_k$ was obtained as a ratio :

$$T(\omega)_k = \frac{V_{o\cdot k} + n(t)}{V_{in\cdot k} + n(t)}$$

and stored in an array along with the corresponding frequency. The digital code was then incremented by a specified amount (corresponding to a given intersample spacing) to obtain the (k+1) th sample point. This procedure was repeated until arrays $\bar{T}(\omega)_k$ and $\bar{f}_k$, $(k=1,2,\ldots n)$ were obtained over the sampling range.

5.0.16.2 Simulation : Data Processing Phase.

At the end of the data acquisition phase, an array of $T(\omega)$ values and a corresponding array of frequencies were obtained. These data samples were then smoothed using the smoothing routine described earlier; the smoothed values were differentiated. An array of first derivatives was obtained in this way. From this array, the peak positive and negative first derivatives and the corresponding (inflection point) frequencies were identified. The resonant frequency

f_0 and the Q factor were calculated from these inflection point frequencies along with their uncertainities.

In studying the VCO jitter , the simulation process was rerun with a different value of f_{Start} in each case and the resulting uncertainities in f_0 and Q were calculated for each case. In studying the noise effects , the simulation process was rerun , as mentioned earlier, with a different S/N level in each run , and the resulting uncertainities in f_0 and Q were calculated as above.

The next section descibes the use of the above procedure in a typical case.

5.0.17 Simulation Case Study.

Consider an experimental setup with :

-a resonator at f_0 =1000 MHz and Q=450

-a calibrated VCO with a tuning characteristic of 14.3 MHz/V;a power/frequency characteristic of 2.95 mW/MHz over the frequencies of operation and an accuracy of ±10 kHz.

-a detector with a sensitivity of 22 mW/mV over the range of operation.

The simulation process described above was then used . The critical components of the experimental system were the VCO characteristics and the noise levels at the detectors.The simulation deals with these aspects. It must be

mentioned that the simulation was intended primarily to study the present experimental system;thus the simulation concentrates on factors deemed to be critical in the experimental arrangement.The contribution of other factors such as quantization noise to the measured inflection points , was considerably smaller;thus , for the present experimental system , this error was approximately 2 kHz , while the error due to the VCO frequency uncertainity was approximately 20 kHz.Since the uncertainity of a function is proportional to the square of the uncertainity of the largest component [23] , it was decided that the quantization noise was negligible.When the VCO frequency uncertainity is comparable to the contribution due to quantization noise , the latter can no longer be ignored.. Since this case study dealt with the case of a VCO with a frequency accuracy of ± 10 kHz , the effects of quantization noise could be considered negligible. The VCO charateristics of interest were :

1. VCO frequency jitter , non-linearity of the tuning characteristic and drift
2. power level variation

The other factor of interest in the simulation was the noise level at the detector and the effect of different signal/noise (S/N) ratios.

Before considering the actual simulation itself , it is useful to consider certain additional aspects.In both the experimental arrangement and the simulation , the uncertain-

ities in f_o and Q factor can be reduced by decreasing the intersample spacing. The intersample spacing is determined by the VCO frequency accuracy. Figure 12 depicts the consequences of this action for a case of a VCO with a frequency accuracy of ±10 kHz.

From Figure 12 , when the VCO is tuned by a voltage V_1 , the output frequency F_1 is obtained with an accuracy of ±10 kHz; thus the actual frequency can be anywhere in the F_{1A} - F_{1B} range. When the VCO is tuned to V_2 , the frequency F_2 is similarly obtained in the F_{2A} - F_{2B} range. Thus , unless the (V_1 - V_2) increment is sufficiently large , V_1 and V_2 may give rise to the same output frequency. It is for this reason that the tuning increment is made large enough to provide a 20-kHz increment between F_1 and F_2 , for the given VCO. Thus the intersample spacing is fixed at 20 kHz.

The ±10 kHz accuracy of the VCO used in this case study was chosen in order to consider the case of the VCO used in the experimental arrangement - the HP8699B RF unit - which has a frequency accuracy of ±10 kHz.

5.0.17.1 Simulation Results : VCO Effects.

As mentioned earlier , the frequencies f_k of the data samples vary not only with the random frequency Δf_k added to them , but , also with the initial frequency f_{Start} used in obtaining f'_k in Figure 10 This was used , as already indi-

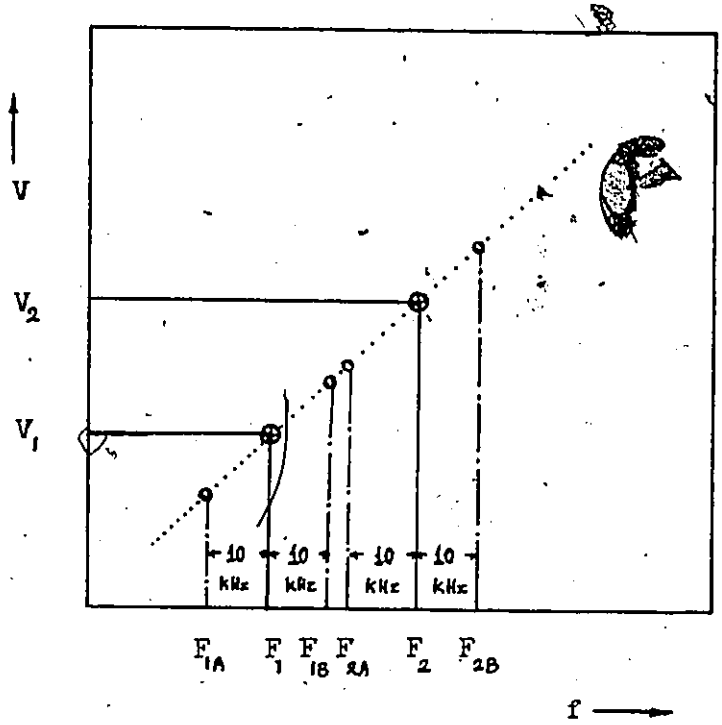

Figure 12: Effects of the VCO frequency accuracy.

cated , in simulating jitter by using the simulation algorithms with a different value of f_{Start} in each run; this caused the sample frequencies f_k to be different in each case (since $f_k = F(f_{Start}, \Delta f_k)$). The other VCO frequency effect , non-linearity of the tuning characteristic , was simulated by the random frequency component Δf_k of the sample frequency f_k .

The numerical first derivative is a function of the transmission loss $T(\omega)$, over a set of 3 or 5 points. Changes in the sample frequencies due to jitter , etc. cause changes in the corresponding transmission loss $T(\omega)$ (for the same digital code) , and therefore , in the numerical values of the first derivatives. These changes in the first derivatives may cause changes in the positions of the peak positive and negative first derivatives , thereby causing changes in f_o and Q factor.

Table 5 shows this phenomenon; in the experiments , the initial frequency f_{Start} was changed in different runs of the simulation , causing changes in the calculated values of f_o and Q factor . The table also shows the resulting uncertainities in f_o and Q factor. The uncertainities were calculated from the f_o and Q factor obtained by identifying the inflection points on the simulated resonance curve and comparing them with the actual f_o and Q factor of the resonator used in the simulation.

TABLE 5

Effects of VCO jitter on the uncertainities of f_0 and Q factor.

VCO initial Freq.(f_{start}) (MHz)	f_0 (Obtained from the Simulation Experiments).	Q	Uncertainities of the Simulatio Experiments.	
			$\frac{\Delta f_0}{f_0}$ (ppm)	$\frac{\Delta Q}{Q}$ (%)
982.78	988.58	488	121	8.44
982.8	988.6	482	101	7.11
982.82	988.6	482	101	7.11
982.83	988.57	538	131	19.6
982.84	988.57	538	131	19.6
982.86	988.57	538	131	19.6

Actual f_0 = 988.7 MHz.

Actual Q =450.

5.0.17.2 Simulation Results : Noise Effects.

A difficulty arises in evaluating the effects of noise alone in this case study. As shown in Table 5 , uncertainities in f_0 and Q factor from the simulation are affected by the sample frequencies f_k , which are in turn affected by the initial frequency f_{Start}. When the intersample spacing is relatively large (20 kHz in this case) , if the inflection points of the actual resonance curve happen to lie close to the sample frequencies f_k , the resulting uncertainities are smaller. Therefore , depending on the value of f_{Start} used , the sample frequencies could lie near or far from the actual inflection points of the curve , causing corresponding changes in the uncertainities in f_0 and Q factor. As long as f_{Start} affects the resulting uncertainities , the effect of noise alone cannot be evaluated. This is because f_{Start} affects the uncertainities more than any changes in the noise level.

If the intersample spacings were smaller , this problem would probably not arise , since the resulting samples would be very close to each other and will hence be less affected by f_{Start}. In the case of the present case study , intersample spacing being 20 kHz , it was decided to carry out the simulation runs with the combined effects of varying S/N ratios and jitter since the latter was going to affect the uncertainities anyway. Table 6 shows the results from this test. From Table 3 , section 4.2.4, it is seen that to mea-

sure a Q factor of 500 , the S/N ratio must at least be 36 dB. Table 6 shows that for a Q factor of 450 , with an S/N ratio of 27 dB no reading can be made.The simulation runs ware carried out at 27 , 35 , 55 and 70 dB since intermediate changes in S/N ratio did not indicate any change.

Two factors become apparent from this study (Table 6).

1. It is difficult to state categorically what the effects of lowering N/S ratios will be (once an acceptable minimum has been achieved , as given in Table 3 for a given Q factor) , since the VCO initial frequency f_{Start} has a larger effect on the resulting uncertainity.One factor which tends to lead to the conclusion that S/N ratios are not too critical to the system performance is the fact that repeated runs at different S/N ratios indicate very little change in the values of the first derivatives and hence the position of the peak positive and negative first derivatives , and therefore in the calculated values of f_0 and Q factor. However , as indicated both by Table 3 and Table 6 a 'threshold' S/N ratio may be required for a given Q factor , as an S/N ratio of less than 33 dB could not be used , since the higher noise level affected the differentiation , and produced numerous positive and negative maxima (instead of one set of maxima), rendering the results unusable.

TABLE 6

Combined effects of varying S/N levels and VCO jitter on the uncertainities of f_o and Q factor.

Actual f_o = 988.7 MHz.

Actual Q = 450.

Intersample spacing = 20 KHz.

VCO initial frequency (f_{Start})(MHz)	Signal level / Noise level (dB)	f_o from Simulation	Q from Simulation	$\frac{\Delta f_o}{f_o}$ (ppm)	$\frac{\Delta Q}{Q}$ (%)
982.78	27	*	*	*	*
	35	988.58	488	121	8.44
	55	988.7	517	0	14.88
	70	988.7	517	0	14.88
982.80	27	*	*	*	*
	35	988.6	482	101	7.11
	55	988.7	550	0	22.22
	70	988.7	550	0	22.22
982.83	27	*	*	*	*
	35	988.56	537	141	19.3
	55	988.72	540	20	20.2
	70	988.73	550	30	22.2

* : Indicates no reading possible.

2. Table 6 also evaluates the uncertainities , which were obtained by comparing the values of f_0 and Q factor calculated from the simulation with the actual f_0 and Q of the resonator used in the simulation. Although zero errors in f_0 are indicated with high errors in Q factor these zero errors are probably due to the occurence of symmetrical errors in the two inflection points so that the resulting errors in f_0 are zero while the errors in the inflection point bandwidth cause the errors in Q factor shown.

Chapter VI

PERFORMANCE

This chapter provides a description of the system performance. In order to verify the basic concept, the system was initially tested at low radio frequencies using an IF transformer as a resonant circuit and then at microwave frequencies using a coaxial resonator. In the first case the inflection points were identified by determining the points on the curve at which the second derivative was zero; this approach was found to be unsuitable however, since noise and VCO instabilities rendered the resulting calculated values of the second derivative unusable. When the system was redesigned at microwave frequencies, the repeatability of the results was still not satisfactory; this led to a study of the theoretical measurement uncertainity and the design of a simulation, where the effects of VCO accuracies and varying signal/noise levels were considered.

The experiments were designed to consider the following aspects:

1. System performance with circuits operating at different frequencies over an octave-bandwidth VCO.
2. System performance with resonant circuits with different Q factors.

It was decided to perform the experiments at different frequencies over an octave-bandwidth VCO in order to study the system performance over widely differing frequencies and to see whether this caused appreciable changes in the measurement uncertainities. The frequencies considered were 990 MHz , 1003 MHz and 1100 MHz , representing a total tuning range of 110 MHz.

It was also decided to test the system over a range of Q factors in order to check the measurement accuracy over the range considered. From a study of system specifications section (4.2.5) , it was found that the system was capable of measuring Q factors in the 50 to 1000 range.

The performance was evaluated on the basis of a series of experiments. Statistical variations of f_o and the Q factor where then calculated. The measurement uncertainities of f_o and the Q factor were calculated using standard deviations.

The experiments were performed under computer control;a command file was used to run a series of experiments continuously , the measured f_o and Q factor being stored on the system disk at the end of each experiment.The values of f_o and Q factor were later used off-line to calculate the mean and standard deviation of the series of experiments .

6.0.18 The Resonant Circuit.

The resonant circuit used in the testing of the system performance was an open-ended coaxial resonator whose f_o and Q factor were variable .The resonant frequency was :

$$f_o = \frac{c}{4l}$$

where ,

f_o is the resonant frequency

c is the velocity of light, , and

l is the length of the inner conductor.

By changing the length l therefore , f_o can be changed.Decreasing the line length increases the frequency.

The Q factor can be changed by adjusting the coupling loops.As was shown in Figs.3 and 4 the resonator can be represented by a series resonant circuit at a voltage anti-node (detuned open position). The source and load impedances can be transformed to the inner loop , the coupling loops acting as transformers , as shown in Fig.4.Thus , at maximum coupling the external impedances transformed to the inner circuit are maximum so that the loaded Q factor is minimum.Decreasing the coupling , therefore , increases the Q factor.

6.0.19 Experimental Results : f_o Variation.

The coaxial resonator was tuned , using a movable plunger ;the resonant frequencies were measured in three sets of experiments , each set consisting of ten repetitive measurements at a single tuning. Tables 7-9 depict the results. The mean values were 990.54 MHz , 1003.48 MHz and 1100.46 MHz.The Q factor changed at higher frequencies (from 430 to 380). The standard deviations of the frequency were of the same order of magnitude , 14-23 kHz , as where those of the Q factors , 8-11.

TABLE 7

Experimental results for a resonator at f_o = 990.54 MHz.

FO:	990.54	Q:	421.87
FO:	990.55	Q:	441.37
FO:	990.54	Q:	439.74
FO:	990.51	Q:	420.32
FO:	990.54	Q:	439.74
FO:	990.52	Q:	429.79
FO:	990.57	Q:	428.24
FO:	990.56	Q:	441.46
FO:	990.56	Q:	438.03
FO:	990.55	Q:	439.74
MEAN FO:	990.54	MEAN Q:	434.0
STD DEV OF FO:			0.0187324
STD DEV OF Q:			8.2345619

TABLE 8

Experimental results for a resonator at f_o = 1003.48 MHz.

FO:	1003.47	Q:	425.79
FO:	1003.50	Q:	445.45
FO:	1003.48	Q:	418.12
FO:	1003.49	Q:	407.84
FO:	1003.48	Q:	415.10
FO:	1003.47	Q:	424.24
FO:	1003.48	Q:	433.79
FO:	1003.49	Q:	433.79
FO:	1003.51	Q:	427.42
FO:	1003.47	Q:	425.79
MEAN FO:	1003.48	MEAN Q:	425.
STD DEV OF FO:			0.013512
STD DEV OF Q:			10.619120

TABLE 9

Experimental results for a resonator at f_o = 1100.46 MHz.

FO:	1100.46	Q:	389.64
FO:	1100.41	Q:	376.91
FO:	1100.47	Q:	375.77
FO:	1100.50	Q:	372.50
FO:	1100.45	Q:	389.64
FO:	1100.48	Q:	375.77
FO:	1100.46	Q:	389.64
FO:	1100.45	Q:	392.01
FO:	1100.47	Q:	378.22
FO:	1100.46	Q:	389.56
MEAN FO:	1100.46	MEAN Q:	386.0
STD DEV OF FO:			0.023302
STD DEV OF Q:			7.682052

It would seem from this that the system performance was

not degraded at higher frequencies.This is quite reasonable since the VCO accuracy is ±10 kHz over the octave- bandwidth of 0.1-2 GHz.The above variations in the system performance can be attributed to variations in the VCO power level with frequency , variations in the detector characteristics with input power and frequency , and variation in the directional couplers with frequency.The resulting changes in the signal levels can cause changes in the signal/noise ratio thereby causing small changes in the calculated derivatives.

6.0.20 Experimental Results : Q factor Variations.

The coupling loops were adjusted to three different positions and the resulting Q factors were measured.Tables 10-12 indicate the results. Table 10 shows the case of maximum coupling;Table 12 that of minimum coupling. Repetitive experiments were performed about thirty times so as to get a better sample set with which to evaluate the statistical variations. In Table 10 with maximum coupling the mean value of f_o was 990.52 MHz while the mean Q factor was 390.9.In Table 12 with minimum coupling , the mean value of f_o was 989.97 MHz while the mean Q factor was 887.4. The standard deviations of the frequency were of the same order in Tables 10-12 , viz.,10-11 kHz.The standard deviations of the Q factor were comparable (Tables 10 and 11) , about 6 , while in Table 12 the standard deviation was 20.The higher value of standard deviation in the latter case was expected

since the uncertainity of measurement was expected to rise with the Q factor , from section 3.3.

Table 13 compares theoretical and experimental uncertainities for the three resonator settings of Tables 10-12 , with Q factors of 380, 415 and 890. The theoretical uncertainties of f_0 were calculated for an f_0 of 990 MHz , while those of Q factor were calculated for Q factors of 381, 415.5 and 888 , using the formulas presented in the uncertainity analysis of section 3.3. The experimental uncertainities were calculated to within three standard deviations (3 SD) from Tables 10-12. As indicated in Table 13 , the theoretical and experimental uncertainites were comparable.

TABLE 10

Experimental results for maximum coupling. The mean values are: f_o = 990.52 MHz and Q = 380.9.

FO:	990.53	Q:	386.2
FO:	990.53	Q:	386.2
FO:	990.52	Q:	386.2
FO:	990.54	Q:	378.5
FO:	990.54	Q:	373.6
FO:	990.52	Q:	381.1
FO:	990.52	Q:	371.2
FO:	990.51	Q:	376.1
FO:	990.51	Q:	378.5
FO:	990.52	Q:	381.1
FO:	990.52	Q:	376.1
FO:	990.50	Q:	376.0
FO:	990.50	Q:	371.2
FO:	990.53	Q:	366.4
FO:	990.51	Q:	383.5
FO:	990.52	Q:	373.6
FO:	990.52	Q:	386.2
FO:	990.51	Q:	386.2
FO:	990.52	Q:	383.6
FO:	990.52	Q:	388.8
FO:	990.53	Q:	386.2
FO:	990.52	Q:	386.2
FO:	990.54	Q:	386.2
FO:	990.53	Q:	386.2
FO:	990.54	Q:	383.6
FO:	990.54	Q:	386.2
FO:	990.53	Q:	386.2
FO:	990.53	Q:	386.2
FO:	990.53	Q:	388.8
FO:	990.52	Q:	373.6
FO:	990.51	Q:	373.6
FO:	990.51	Q:	376.1
MEAN FO:	990.52		
MEAN Q:	380.9		
STD DEV OF FO:			0.0114
STD DEV OF Q:			6.2296

TABLE 11

Experimental results for reduced coupling. The mean values are : f_0 = 990.59 MHz and Q = 415.5.

F0:	990.59	Q:	433.1
F0:	990.59	Q:	417.3
F0:	990.60	Q:	405.5
F0:	990.57	Q:	420.3
F0:	990.59	Q:	414.2
F0:	990.59	Q:	408.3
F0:	990.57	Q:	408.3
F0:	990.60	Q:	417.3
F0:	990.56	Q:	411.3
F0:	990.58	Q:	426.6
F0:	990.59	Q:	405.5
F0:	990.58	Q:	417.3
F0:	990.58	Q:	420.3
F0:	990.58	Q:	411.3
F0:	990.60	Q:	405.5
F0:	990.60	Q:	417.3
F0:	990.59	Q:	420.3
F0:	990.58	Q:	420.3
F0:	990.58	Q:	417.1
F0:	990.58	Q:	408.3
F0:	990.61	Q:	420.3
F0:	990.61	Q:	408.3
F0:	990.59	Q:	408.3
F0:	990.60	Q:	417.3
F0:	990.61	Q:	420.3
F0:	990.60	Q:	417.3
F0:	990.59	Q:	423.4
F0:	990.61	Q:	411.3
F0:	990.60	Q:	417.3
F0:	990.59	Q:	417.3
F0:	990.61	Q:	411.3
F0:	990.60	Q:	417.3
MEAN F0:	990.59		
MEAN Q:	415.5		
STD DEV OF F0:			0.011/
STD DEV OF Q:			6.403

TABLE 12

Experimental results with the least coupling. The mean values are: f_0 =989.97 MHz and Q=887.4.

F0:	989.98	Q:	892.7
F0:	989.98	Q:	892.7
F0:	989.96	Q:	892.6
F0:	989.96	Q:	892.6
F0:	989.97	Q:	906.8
F0:	989.98	Q:	877.0
F0:	989.99	Q:	892.6
F0:	989.96	Q:	892.6
F0:	989.98	Q:	892.7
F0:	989.95	Q:	878.8
F0:	989.98	Q:	892.7
F0:	989.97	Q:	828.0
F0:	989.97	Q:	892.7
F0:	989.96	Q:	865.4
F0:	989.98	Q:	892.7
F0:	989.98	Q:	906.9
F0:	989.97	Q:	840.2
F0:	989.96	Q:	892.6
F0:	989.96	Q:	892.6
F0:	989.98	Q:	906.9
F0:	989.97	Q:	892.7
F0:	989.98	Q:	906.9
MEAN F0:	989.97		
MEAN Q:	887.4		
STD DEV OF F0:			0.0104
STD DEV OF Q:			17.8510

TABLE 13

Comparison of theoretical and experimental uncertainities

Resonator	f_o (MHz)	Q	Maximum Theoretical Uncertainity.		Experimental Uncertainity. (3 SD)	
			$\frac{\Delta f_o}{f_o}$ (ppm)	$\frac{\Delta Q}{Q}$ (%)	$\frac{\Delta f_o}{f_o}$ (ppm)	$\frac{\Delta Q}{Q}$ (%)
1	990.0	381	50	3.3	34.2	4.89
2	990.0	415.5	50	3.6	35.2	4.67
3	990.0	888	50	7.7	39.4	6.7

6.0.21 A low Q Resonator.

The measurement system was also tested with another resonator with a very low Q factor of approximately 10.The resonator was a 50Ω microstrip transmission line ;the coupling was such that the outer jacket was connected to the ground plane of the microstrip while the inner conductor was connected to the transmission line.The device acts as an absorption type resonator the transmitted power being a minimum at the resonant frequency of 520 MHz.

The measurement was not very accurate as indicated in Table 14. From Table 3 , a Q factor of 10 requires a signal/noise ratio of 70 dB , which was not available in this case.Also the VCO accuracy was ±10 kHz.These factors combined to produce random positive and negative peaks in the calculated first derivatives , making the results unreliable and possibly wrong.In order to measure a Q factor of this order of magnitude,the factors that need to be considered are noise levels at the output , VCO accuracies and A/D as well as D/A resolution.These aspects will be considered in more detail later.

TABLE 14

Experimental results with a low Q resonator. The mean values are : f_0 = 514.66 MHz and Q = 10.3.

F0:	515.09	Q:	10.7
F0:	516.17	Q:	11.5
F0:	514.80	Q:	11.2
F0:	514.64	Q:	9.7
F0:	514.95	Q:	9.7
F0:	515.40	Q:	9.7
F0:	514.49	Q:	10.0
F0:	512.84	Q:	10.1
F0:	514.97	Q:	11.3
F0:	514.34	Q:	10.6
F0:	515.14	Q:	10.1
F0:	514.97	Q:	9.8
F0:	512.77	Q:	9.7
F0:	514.97	Q:	11.4
F0:	514.81	Q:	9.7
F0:	514.98	Q:	9.7
F0:	514.98	Q:	10.5
F0:	514.88	Q:	9.7
F0:	514.98	Q:	11.5
F0:	514.95	Q:	9.7
F0:	515.05	Q:	11.7
F0:	514.97	Q:	9.7
F0:	512.79	Q:	11.3
F0:	514.99	Q:	9.7
F0:	515.43	Q:	10.0
F0:	514.99	Q:	9.7
F0:	514.99	Q:	9.7
F0:	514.37	Q:	10.1
F0:	514.92	Q:	10.6
F0:	514.30	Q:	10.1
F0:	516.69	Q:	10.9
F0:	514.36	Q:	10.1
MEAN F0:	514.66		
MEAN Q:	10.3		
STD DEV OF F0:			0.9198
STD DEV OF Q:			0.6764

6.0.22 Analysis of the System Performance.

As indicated in Tables 7-14 , the experimental system was tested at different f_o and different Q . This was done with a view to obtaining a better basis on which to consider the system performance. The simulation as well as the uncertainity analysis also helped in quantifying system performance. From a consideration of the overall system (including the experimental system , the simulation and the uncertainity analysis) , it is possible to :

1. Evaluate the usefullness of the measurement system for the intended areas of application , and
2. Consider the factors which affect the achieved experimental accuracies.

These aspects are considered below.

6.0.22.1 Suitability of the Measurement System for the Intended Areas of Application.

The measurement system was designed to be used primarily for monitoring changes in f_o and Q factor , which are needed in measuring ϵ' and ϵ'' through cavity perturbation techniques. This requires :

1. Response times on the order of 2-3 s , and
2. Typical measurement accuracies of about 0.25% for a Q factor of 400 , so that changes of 1 in Q factor can be measured.

The present measurement system takes about 400 ms for the data acquisition phase;the complete measurement takes about 15 s.All the programming was done in FORTRAN.It is felt that optimising the main program and programming in the assembly language of a given machine would improve the system speed considerably so as to permit system response in real-time.

As for the other factor , the measurement accuracy , the present measurement uncertainity is approximately 5% for a Q factor of 400.The factors responsible for the achieved accuracy will be dealt with in the next section.This work having provided a good indication of these factors , it is felt that the measurement accuracies can be improved relatively easily , so that accuracies of 0.25% at a Q factor of 400 are feasible.

6.0.22.2 Factors Affecting Measurement Accuracy.

As indicated both by the uncertainity analysis (section 3.3) and the simulation case study (section 5.0.18) ,the largest component in the uncertainity of the measured inflection points is the VCO frequency accuracy of ±10 kHz.Drift in the VCO frequency is negligible since the measurement is carried out very fast;power level variation over the tuning bandwidth is also small for high Q factors (where the inflection point bandwidth is small).The effects of D/A converter resolution , A/D converter quantization error and

counter uncertainity are small.Thus it would seem that the accuracy of the measurement could be improved considerably by obtaining a VCO with a better frequency accuracy.

The effects of the VCO frequency accuracy were noticed very clearly during the performance of the experiments.The specification sheet of the VCO - the HP8699B - indicate that the frequency accuracy is ±10 kHz.Thus the VCO attains a frequency corresponding to a specified tuning voltage with an accuracy of ±10 kHz.As was explained in the simulation case study (section 5.0.18), it is not possible to tune the VCO in voltage increments that cause changes in VCO frequency of less than 20 kHz.There are, in addition ,the effects of the D/A converter resolution and A/D converter quantization error.The intersample spacing must take all these factors into account.The spacing was thus selected as 25 kHz.As mentioned earlier , the intersample spacing affects the accuracy with which the inflection points of the curve can be determined. The major component in fixing the intersample spacing is the VCO accuracy .If a more accurate VCO such as a frequency synthesizer with a frequency accuracy of.1 ppm at 1 GHz is used , the intersample spacing could be reduced considerably , so that the inflection points on the curve can be identified more accurately.

Noise at the outputs of the detector is another factor that affects the measurement accuracy , especially at low Q

factors. In the case of resonant structures with low Q factors, the voltage differences between adjacent samples is small; thus a number of samples might have essentially the same output voltage. Unless, therefore, bandlimited signal conditioning amplifiers and high resolution converters are used, the converted levels will be the same for a number of samples. If the A/D resolution cannot be improved, larger differences between adjacent sample voltages can be obtained by increasing the intersample spacing. This latter approach, however, affects the accuracy with which the inflection points can be determined, and hence the accuracy with which f_o and Q factor can be calculated. High VCO frequency uncertainity further aggravates this problem. These problems were found to be particularly troublesome in measuring the Q factor of the resonant structure with a Q factor of approximately 10 and f_o of 520 kHz mentioned in an earlier section.

6.0.23 Conclusion.

This work has dealt with the development of a new measurement system. The accuracies obtained were 40 ppm in frequency and nearly 7% in Q factor for a Q factor of 890, which are comparable to measurement accuracies obtained from other systems. The factors causing the experimental errors have been investigated. This study of experimental errors has indicated that the measurement uncertainity is mainly dependant on :

1. VCO frequency uncertainity
2. The noise levels at the detector outputs
3. A/D and D/A resolution.

These are seen to be the factors important in selecting the intersample spacing and therefore in locating the inflection points on the curve accurately. The major component in the measurement uncertainity is the VCO frequency uncertainity. Improving the VCO frequency uncertainity would improve the accuracy of the measurement, as indicated earlier.

In order to reduce the uncertainity with which the inflection points could be determined, other approaches were tried. Thus, once the peak derivative maxima had been identified, a second degree polynomial was fitted to the derivatives around the peak, and the derivative of this polynomial was obtained; the inflection points would then be identified as the points at which this derivative became zero. The values obtained were however random positive and negative values. It is felt, nevertheless, that this approach deserves further investigation.

Another possible approach is to consider fitting a least-squares polynomial to the n sample points, using the equation of the transmission loss $T(\omega)$ given earlier. This approach poses further problems, since there are two unknowns to be determined, viz., Q and resonant frequency, from the sample points.

Modifying the measurement system in the above manner to reduce the measurement errors would satisfy the intended design objectives of high accuracy and total automation. The system would then be suitable for a wide range of applications.

Chapter VII

CONCLUSIONS.

A new approach to the measurement of resonant frequency and Q factor was investigated in this work. The need for accurate measurement of resonant frequency and Q factor arises from their use in monitoring dielectric properties of materials. The system can also be used for other industrial and biological applications .Quality factors Q in the 10-1000 range can be measured at radio and microwave frequencies.

A study of the state-of-the-art in Q factor measurements indicated that the majority of the available systems were dependant on the detector and resonator characteristics and only one was totally automated.It was therefore decided to design a measurement system that would be very accurate , totally automated and independant of detector , resonator and VCO characteristics.This led to the development of the present measurement system . In this system the inflection points of the resonance curve are identified by a process of mathematical evaluation and the resonant frequency as well as Q factor are calculated from the inflection point frequencies.

The measurement system operates in two phases : a data acquisition phase and a data processing phase. In the data acquisition phase , the resonator response is captured in real-time ;this data are then manipulated at a slower rate in the data processing phase. A PDP 11/34 minicomputer is used for overall system control and for data processing. The resonator response is monitored continuously , a printout of the Q factor and resonant frequency being available at the end of each measurement.

In the following sections , the various stages in the execution of this project are described. Once formulas for resonant frequency and Q factor in terms of the inflection point frequencies were derived , the system was tested at radio frequencies , an IF transformer being used as the resonant circuit. The inflection points were identified by obtaining the numerical second derivative from the data points. The second derivatives obtained were unusable because of noise and VCO inaccuracies , so it was decided to identify the inflection points by identifying the peak positive and negative first derivatives instead.

At this stage , an uncertainity analysis was carried out in order to obtain a theoretical basis on which to evaluate the system performance. Further analysis was then made to define the system specifications in terms of the range of measurable Q factors for a given range of frequencies and for a specified hardware.

The system was then reconfigured at microwave frequencies with the digital I/O lines 0-11 of the PDP 11/34 being used to supply the input code to the D/A converter driving the VCO , a TEXSCAN model VTO-100 . The IF transformer was replaced by a coaxial resonator.

A simulation of the system was then designed to study the effects of the VCO characteristics and signal/noise ratios on measurement uncertainities. The simulation showed that the VCO frequency uncertainity is the largest component of the measurement uncertainity , once a specified minimum signal/noise ratio is available for a given Q factor.

From this study of the theoretical analysis and the simulation results , the system was redesigned;the AA 11-K D/A converter module having by then become available on the PDP 11/34 , it was used to replace the external D/A converter.Bandlimited signal conditioning amplifiers were used to transform the detector outputs to the dynamic range of the A/D converters.A stability study of the VCO had indicated that the frequency uncertainity of the VTO-100 was ±35 kHz , so this was replaced with the HP8699B , which has a frequency uncertainity of ±10 kHz.

A whole series of experiments were then performed on the coaxial resonator. The resonant frequency and Q factor of the resonator being variable , the measurements were made at different values of these parameters.The results obtained

from these measurements were tabulated along with the statistical variations of the resonant frequency and Q factor. From this, it was found that the measurement uncertainity in the resonant frequency (3 SD) was 40 ppm while that of the Q factor was nearly 7% for a Q factor of 890. The results were then analyzed and interpreted. Various possible causes for the achieved measurement uncertainities were considered. It was concluded that the main component of the uncertainity of the measured inflection point frequency was the uncertaintiy of the VCO.

Higher accuracies on the order of 2 ppm in the resonant frequency can be achieved with a more accurate VCO such as a frequency synthesizer. This would provide an uncertainity of 0.3 % in the Q factor for a Q factor of 1000. If, on the other hand, a portable, relatively cheap instrument is envisaged, the system could be built with microprocessors and off- the-shelf microwave components, some form of jitter control being used on the VCO.

Other approaches to reducing the uncertainity of the measured frequency include fitting a second degree curve (a parabola) to the derivative values arcund the maxima; the derivative of this curve can then be obtained and the inflection point identified as the zero-crossing point. Also, least-squares curve fitting using the known equation of the transmission response $T(\omega)$ to the sample set can be investigated.

When the system was first designed it was intended , as mentioned earlier , to be very accurate , totally automated and independant of the detector and resonator characteristics as well as the VCO. As was seen in the preceding chapters , not all the intended objectives were achieved.Some of the problems that arise in the development of a new measurement or instrumentation system became apparent in the endeavour to achieve these objectives.A few of these problems were interrelated.Thus high accuracy could not be achieved without some form of jitter control being used on the VCO.Other possible sources of error such as frequency drift , power variation , etc. were seen to be less important.Independence of the measurement uncertainities from the detector and resonator characteristics were attained and the measurement system was totally automated.

Even though not all of the intended objectives were achieved , the causes for this were at least enumerated.Possible methods to overcome these problems were also discussed.In spite of these problems , it is seen that the measurement accuracies were comparable to those attained by other measurement systems.It is felt , in addition , that solving the problems in the manner indicated will improve the measurement accuracies considerably.It can be stated therefore , that this measurement system bears a potential to be very useful in a wide range of applications.

****

BIBLIOGRAPHY

1) J. Markowski ,A.D. MacDonald and S.S.Stuchly ,"The Dynamic Response of a Resonant Frequency Tracking System ",IEEE Trans. Instrum. Meas.,Vol. IM-26,No.3,pp.231-237,Sept. 1977.

2) S.S.Stuchly , M.A.Stuchly and B.Carraro ,"Permittivity Measurements in a Resonator Terminated by an Infinite Sample", IEEE Trans. Instrum Meas.,Vol. IM-27,No.4,pp.436-439,Dec. 1978.

3) M.Sucher and J.Fox , Handbook of Microwave Measurements, Vol. II ,3rd ed. Brooklyn , N.Y.: Polytechnic Press,1963,pp.417-493.

4) E.L.Ginzton , Microwave Measurements. New York : McGraw Hill , 1957 , pp. 391-434.

5) K. Francis , " The Accurate Measurements of High Q factors at Frequencies upto 1GHZ ", Electron. Ind. (GB) ,4(6),pp.33-35 , June 1978.

6) I. Kneppo , "Comparison Method of Measuring Q of Microwave Cavities ", IEEE Trans. Microwave Theory & Tech.,MTT 25(5), pp.423-426, May 1977.

7) A.L.Cullen and J.A. Davies ," New System for Microwave Q factor Measurement ", IEE J. Microwaves,Opt. and Accoust., Vol. 2,No.3, pp.77-84 , May 1978.

8) I. Kneppo ," Intergration Method of Measuring Q of Microwave Resonators " ,IEEE Trans. on Microwave Theory & Tech.,Vol. MTT-26, No.2,pp.131 , Feb.1978.

9) N.D.J.Miller ,"The Automatic Measurement of Resonator Q factor", J. Physics E : Sci. Instrum. ,Vol. 11 ,pp.185-186 , Mar.1978.

10) M.Ney and F.Gardiol ," Automatic Monitor for Microwave Resonators ",IEEE Trans. Instrum. Meas. , Vol.IM-26 ,No.1 ,pp.10-13 ,Mar.1977.

11) C.E.Eugene and B.Mollet ," Automatic Measurement of Microwave Cavity Parameters using Stable Sampled Control Loops ",Electronics Letters ,Vol.8,No.17,pp.434-436, 24th Aug. 1972.

12) M.Linzer and D.P.Stokesberry ," A Frequency-Lock Method for the Measurement of Q factors of Reflection and Transmission Resonators ", IEEE Trans. Instrum. Meas. , Vol. IM-22 ,No.1 ,pp.61-77 , March 1973.

13) V.P.Chirkov and A.A.Kozak ," A Digital Q Meter for Tuned Circuits" ,
Izmeritel'naya Tekhnika , No. 11 , Nov.1973 , pp. 62-63. Also available from Consultants Bureau , Plenum Publishing Corporation, 227 West 17th Street , New York , N.Y. 10011.

14) V.Popovic , " An Automatic Digital Q Meter : New Approach to the Digital Measurement of Magnification Factor " ,IEEE Trans. Instrum. Meas. , Vol. IM-27 , No. 2 ,pp.169-171,June 1978.

15) C.Akyel , P.G.Bosisio and G.April ," An Active Frequency Technique for Precise Measurements on Dynamic Microwave Cavity Perturbations ", IEEE Trans. Instrum. Meas. ,Vol. IM-27, No.4, pp.364-368 , Dec.1978.

16) C.Akyel and R.G.Bosisio , " Wide-Range Dynamic Complex Dielectric Constant Measurements using Microprocessor Control Techniques " , IEEE Trans. Instrum. Meas., Vol. IM-27 ,No.4, pp.272-278 , Dec.1979.

17) William S.Dorn and Daniel D.McCracken , Numerical Methods With FORTRAN Case Studies . John Wiley & Sons , Inc. , 1972 , pp.65-90,219-234 and 267-330.

18) A.Papoulis , Probability Random Variables and Stochastic Processes , McGraw Hill , Inc. , 1965 , pp.261-270.

19) IBM Application Programs , System/360 Scientific Subroutine Package , (360A-CM-03X) version III , IV ed. , 1968 ,pp.253-255 and 319-322.

20) Navigational Technology Ltd., Instruction Manual , 4000 Series Electronic Counters.

21) Hewlett-Packard , Operating & Service Manual , FF Unit 8699B , 1969.

22) Digital Equipment Corporation , FSX-11M I/O Drivers Reference Manual , 1977.

23) J.P.Holman , Experimental Methods for Engineers , McGraw Hill , 1978 , pp.1-[illegible]0.

24) A.M.Colella ,M.J.O'Sullivan and D.J.Carlino , Systems Simulation , Lexington Books , 1974 , pp.1-25.

25) A.L.Freedman and P.A.Lees , Real-Time Computer Systems , Crane, Russak and Co.,Inc.,1977,pp.1-160.

26) Digital Equipment Corporation ,PDP 11/34 System User's Manual , 1977.